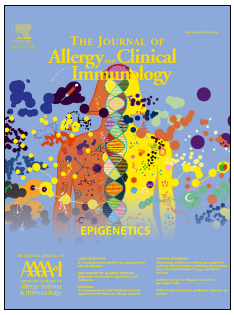
Journal Pre-proof



Epidermal mTORC2 controls lipid synthesis and filaggrin processing in epidermal barrier formation

Xiaolei Ding, PhD, Sebastian Willenborg, PhD, Wilhelm Bloch, PhD, Sara A. Wickström, MD, PhD, Prerana Wagle, MSc, Susanne Brodesser, PhD, Axel Roers, MD, Alexander Jais, PhD, Jens C. Brüning, MD, Michael N. Hall, PhD, Markus A. Rüegg, PhD, Sabine A. Eming, MD

PII: S0091-6749(19)31029-2

DOI: https://doi.org/10.1016/j.jaci.2019.07.033

Reference: YMAI 14119

To appear in: *Journal of Allergy and Clinical Immunology*

Received Date: 25 January 2019

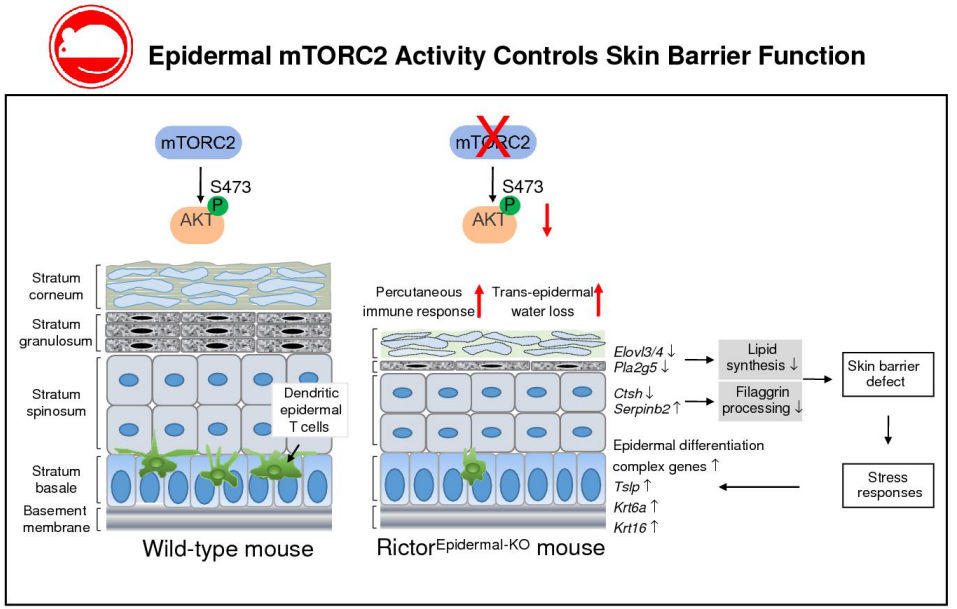
Revised Date: 21 June 2019

Accepted Date: 8 July 2019

Please cite this article as: Ding X, Willenborg S, Bloch W, Wickström SA, Wagle P, Brodesser S, Roers A, Jais A, Brüning JC, Hall MN, Rüegg MA, Eming SA, Epidermal mTORC2 controls lipid synthesis and filaggrin processing in epidermal barrier formation, *Journal of Allergy and Clinical Immunology* (2019), doi: https://doi.org/10.1016/j.jaci.2019.07.033.

This is a PDF file of an article that has undergone enhancements after acceptance, such as the addition of a cover page and metadata, and formatting for readability, but it is not yet the definitive version of record. This version will undergo additional copyediting, typesetting and review before it is published in its final form, but we are providing this version to give early visibility of the article. Please note that, during the production process, errors may be discovered which could affect the content, and all legal disclaimers that apply to the journal pertain.

© 2019 Published by Elsevier Inc. on behalf of the American Academy of Allergy, Asthma & Immunology.



Journal Pre-proof

Journal Pre-proof

Epidermal mTORC2 controls lipid synthesis and filaggrin processing in epidermal barrier formation

Xiaolei Ding, PhD [1,2], Sebastian Willenborg, PhD,[1], Wilhelm Bloch, PhD [3], Sara A. Wickström, MD, PhD [4,5,6,7], Prerana Wagle, MSc [7], Susanne Brodesser, PhD [7], Axel Roers, MD [8], Alexander Jais, PhD [9], Jens C. Brüning, MD [2,7,9], Michael N. Hall, PhD [10], Markus A. Rüegg, PhD [10], Sabine A. Eming, MD [1,2,7]

[1]Department of Dermatology, University of Cologne, Kerpenerstr. 62, 50937 Cologne, Germany

[2]Center for Molecular Medicine Cologne (CMMC), University of Cologne, 50931 Cologne, Germany

[3]Department of Molecular and Cellular Sport Medicine, German Sport University Cologne, 50933 Cologne, Germany

[4]Paul Gerson Unna Group 'Skin Homeostasis and Ageing', Max Planck Institute for Biology of Ageing, 50931 Cologne, Germany

[5]Helsinki Institute of Life Science, Biomedicum Helsinki, University of Helsinki, FI-00014 Helsinki, Finland

[6]Wihuri Research Institute, Biomedicum Helsinki, University of Helsinki, FI-00014 Helsinki, Finland

[7]Cluster of Excellence Cellular Stress Responses in Aging-associated Diseases (CECAD), University of Cologne, 50931 Cologne, Germany

Journal Pre-proof

Journal Pre-proof

[8]Institute for Immunology, Medical Faculty Carl Gustav Carus, TU Dresden, 01307 Dresden, Germany

[9]Max Planck Institute for Metabolism Research, Gleueler Strasse 50, 50931 Cologne, Germany

[10]Biozentrum, University of Basel, CH-4056 Basel, Switzerland

Corresponding author:

Sabine A. Eming, MD

Professor of Dermatology

Department of Dermatology

University of Cologne

Kerpenerstr. 62

50937 Cologne

Germany

Phone: ++49-221-4783196

Fax: ++49-221-4785949

E-mail: sabine.eming@uni-koeln.de

Conflict of interest statement:

The authors have declared that no conflict of interest exists.

Journal Pre-proof

Journal Pre-proof

Abstract

Background: Perturbation of epidermal barrier formation will profoundly compromise overall skin function, leading to a dry and scaly, ichthyosis-like skin phenotype, which is the hallmark of a broad range of skin diseases, including ichthyosis, atopic dermatitis, and a multitude of clinical eczema variants. An overarching molecular mechanism that orchestrates the multitude of factors controlling epidermal barrier formation and homeostasis remains to be elucidated.

Objective: Here we highlight a specific role of mammalian target of rapamycin complex 2 (mTORC2) signaling in epidermal barrier formation.

Methods: Epidermal mTORC2 signaling was specifically disrupted by deleting *Rictor,* encoding an essential subunit of mTORC2 in mouse epidermis (Ric^{EKO}). Epidermal structure and barrier function were investigated by a combination of gene expression, biochemical, morphological and functional analysis in Ric^{EKO} and control mice.

Results: Ric^{EKO} newborns displayed an ichthyosis-like phenotype characterized by dysregulated epidermal *de novo* lipid synthesis, altered lipid lamellae structure, and aberrant filaggrin processing. Despite a compensatory transcriptional epidermal repair response, the protective epidermal function was impaired in Ric^{EKO} mice as revealed by increased transepidermal water loss, enhanced corneocyte fragility, decreased dendritic epidermal T cells, and an exaggerated percutaneous immune response. Restoration of Akt-Ser473 phosphorylation in mTORC2-deficient keratinocytes by expression of constitutive Akt rescued filaggrin processing.

Conclusion: Our findings reveal a critical metabolic signaling relay of barrier formation where epidermal mTORC2 activity controls filaggrin processing and *de novo* epidermal

lipid synthesis during cornification. Our findings provide novel mechanistic insights into epidermal barrier formation and could open up new therapeutic opportunities to restore defective epidermal barrier conditions.

Key words: Epidermal barrier, mTORC2, rictor, ichthyosis, filaggrin, epidermal lipid synthesis

Abbreviations used

ACD:	Allergic contact dermatitis
AD:	Atopic dermatitis
CTSH:	Cathepsin H
DETCs:	Dendritic epidermal T cells
EDC:	Epidermal differentiation complex
FLG:	Filaggrin gene
FFA:	Free fatty acids
γδ-TCR:	γδ-T cell receptor
GSEA:	Gene set enrichment analysis
HPTLC:	High performance thin layer chromatography
IV:	Ichthyosis vulgaris
ICD	Irritant contact dermatitis
Krt:	Keratin
LB:	Lamellar body
Lor:	Loricrin
mTORC1/2:	Mammalian target of rapamycin complex 1/2
myr-AKT:	Myristoylated Akt1
Rictor:	Rapamycin-insensitive companion of TOR
Ric^{EKO}:	Epidermis-specific homozygous Rictor deletion
RNA-seq:	RNA-Sequencing
SB:	Stratum basale
SC:	Stratum corneum
SG:	Stratum granulosum
SS:	Stratum spinosum
TEM:	Transmission electron microscopy
TSLP:	Thymic stromal lymphopoietin
TEWL:	Transepidermal water loss

Capsule Summary (35 words)

An overarching molecular mechanism that orchestrates the multitude of factors controlling epidermal barrier formation remains to be elucidated. Here, we highlight a specific role of mTORC2 signaling in epidermal barrier function.

Key Messages

- The Ric^{EKO} mouse develops an ichthyosis-like phenotype and might serve as a new preclinical disease model for studying epidermal barrier defects at the molecular level.
- Altered mTORC2 activity may represent a predisposing factor for skin disorders associated with disrupted epidermal barrier function.

Journal Pre-proof

Journal Pre-proof

Introduction

The epidermis is a stratified squamous epithelium that provides a life-sustaining permeability barrier preventing water loss and protecting the body from a plethora of physical and chemical insults as well as pathogenic microorganisms [1]. Perturbation of epidermal barrier function will profoundly compromise overall skin barrier function, frequently leading to a dry and scaly, ichthyosis-like skin phenotype, which is the hallmark of a broad range of skin diseases, including ichthyosis, atopic dermatitis (AD), and a multitude of clinical eczema variants associated for example with diabetes mellitus or aging [2-4]. Quality of life is frequently negatively affected and patients are also at high risk for associated morbidity and mortality [5]. The molecular mechanisms regulating proper barrier function and maintenance are not yet understood, and were the aim of this study.

The epidermal barrier function is acquired and maintained by a tightly regulated keratinocyte differentiation process, known as cornification. The innermost mitotically active cell layer, the stratum basale (SB), undergoes continuous proliferation and differentiation, providing cells to the above stratum spinosum (SS), stratum granulosum (SG), and the stratum corneum (SC). The outermost SC makes up most of the permeability barrier. The SC consists of flattened, anuclear and keratin-filled corneocytes embedded in an intercellular lipid-rich matrix composed of ceramides, cholesterol, and free fatty acids (FFA) in an acidic environment [2, 6]. Perturbation of cornification will profoundly compromise skin barrier function [2, 6].

Genetic analyses have established a strong link between genetic defects and skin barrier disorders in both humans and mice, providing the basis for the current

understanding of molecular networks orchestrating cornification [7]. Of particularly importance was the discovery of the loss-of-function mutations in the filaggrin (*FLG*) gene, the cause of the most common genodermatosis, namely ichthyosis vulgaris, which is characterized by dry, scaly skin [8-9]. Ichthyosis vulgaris has been identified as a predisposing factor for the development of AD, the most common chronic inflammatory skin disease, affecting up to 20% of children and 7-10% of adults [10]. However, a significant number of AD patients have no *FLG* mutations and recent human genetic studies suggest that also a reduction of profilaggrin at the protein level can lead to skin barrier defects suggesting that other mechanisms and candidate molecules may regulate profilaggrin expression and proteolytic processing [9, 11]. Further, the identification of mutations in diverse *Elovl* genes in mouse and pediatric AD patients, encoding very-long-chain fatty acid elongases revealed a central role for *de novo* ceramide synthesis in cornification and proper epidermal barrier function [1,10, 12-14]. In addition, *Pla2g5* activity catalyzes FFA synthesis, and has been shown to be critical in epidermal barrier formation [15]. However, the overarching molecular mechanisms that orchestrate the multitude of factors controlling keratinocyte fate and cornification are not known [16-17].

Recently, we identified the serine/threonine protein kinase mammalian (also known as mechanistic) target of rapamycin (mTOR) as an essential regulator of epidermal differentiation and barrier formation in embryonic development [18-19]. Here we hypothesized that mTORC2 plays a critical role in postnatal epidermal barrier assembly and maintenance. mTOR is a central regulator of cell growth and metabolism, and is evolutionarily highly conserved [20-21]. mTOR assembles in two structurally and functionally distinct, multi-protein complexes, referred to as mTORC1 and mTORC2 [20-21].

131 The Rictor (rapamycin-insensitive companion of TOR) protein is an essential and specific
132 subunit of mTORC2. Growth factors are able to stimulate mTORC2 kinase activity, and
133 activated mTORC2 phosphorylates several members of the AGC kinase family, including
134 AKT, specifically at Ser473 (AKT-pSer473) to control cell metabolism and cytoskeleton
135 organization [22-23]. In keratinocyte differentiation, AKT activity is induced, regulating
136 filaggrin expression and processing [24-25]. Interestingly, a recent study showed that
137 increased Raptor expression, the regulatory associated protein of mTORC1 correlates
138 with reduced AKT activity and filaggrin expression in the skin of AD patients [26]. In this
139 study we assessed the role of epidermal mTORC2 in postnatal skin barrier function by
140 inactivating *Rictor* in the epidermis in mice. We show that mTORC2 promotes non-
141 redundant functions for proper cornification via regulation of epidermal lipid metabolism
142 and filaggrin processing. Our findings could suggest a new therapeutic strategy to
143 regulate epidermal barrier function and to prevent complications in patients with dry skin
144 diseases.
145

Journal Pre-proof

Methods

Mice

Epidermal-specific *Rictor* knockout mice (C57BL/6) were generated by crossing mice carrying loxP-flanked *Rictor* alleles with a Cre-transgenic strain expressing Cre recombinase under control of the human K14 promoter (Supplemental Figure 1A) [18]. Littermates that either lacked Cre or expressed Cre but carried a heterozygous loxP-flanked *Rictor* allele served as controls. Genotyping was performed as previously described [18]. Mice were maintained and bred under standard pathogen-free conditions. All procedures were approved by the North Rhine-Westphalian State Agency for Nature, Environment, and Consumer Protection and the University of Cologne.

Histological analysis

Skin tissues were fixed in 4% PFA, embedded in paraffin, and sectioned (10 µm). Hematoxylin and eosin staining was performed following a standard procedure [27]. Images were analyzed using a light microscope (Leica DM4000B, Leica Microsystems, Wetzlar, Germany).

Separation of epidermis from mouse back skin

The subcutaneous fat tissue was mechanically dissected from excised back skin. The epidermis was separated from the dermis after floating skin biopsies in 0.5 M ammonium thiocyanate (NH_4SCN) in phosphate buffer, pH 6.8 (0.1 M NH_2HPO_4, 0.1 M KH_2PO_4) for 30 min on ice, epidermis side up. The epidermis was used for either RNA isolation, biochemical analysis, or immunostaining.

169

170 **Immunostaining**

171 For immunohistochemical and immunofluorescence staining, cryosections from Optimal
172 Cutting Temperature compound (OCT, Tissue Tek) embedded tissues were fixed (4%
173 PFA or in methanol), blocked (10% normal goat serum in PBS), and incubated with
174 primary antibodies (diluted in blocking buffer) overnight at 4°C. Bound primary antibody
175 was detected by incubation with peroxidase-conjugated (EnVision System, Dako)
176 secondary antibody followed by incubation with peroxidase substrate (Sigma) or Alexa-
177 Fluor 488- or Alexa Fluor 594-conjugated antibodies (Invitrogen). Nuclei were
178 counterstained with hematoxylin or 4,6-diamidino-2-phenylindole (DAPI, Invitrogen).
179 After washing, slides were mounted in mounting medium. For whole-mount staining,
180 epidermis was separated from ears as described above. Epidermal sheets were fixed by
181 acetone and stained with anti-γδ-TCR antibody. Images were taken with a Zeiss Meta 710
182 Confocal Microscope or KEYENCE Fluorescence Microscope (BZ-9000). Antibody
183 information can be found in Supplemental Table 1. For quantification of pAkt-S473
184 staining, three representative HPFs/section were quantified using ImageJ software
185 (https://imagej.nih.gov/ij/index.html) as described previously[27]. Findings are expressed as
186 the percentage of pAkt-S473 stained areas within the ear epidermis. Numbers of
187 inflammatory cells were determined by counting positively stained cells in five
188 representative HPFs (400x)/section. Analyses were performed in a blinded manner by
189 two independent investigators.

190

191 **Transmission electron microscopy**

Skin tissues were isolated and fixed in buffer (2% paraformaldehyde, 2% glutaraldehyde, 0.1M cacodylate buffer at pH 7.35) and postfixed with ruthenium tetroxide. Tissue embeeding and ultrathin section preparation were done as previously described [28].

Flow cytometry and cell sorting

For analysis of immune cells, single-cell suspensions of skin from control and Ric^{EKO} were prepared by a combination of enzymatic digestion (Liberase Blendzyme, Roche Applied Science) and mechanical disruption (Medimachine System, BD Biosciences) as previously described [28]. For flow cytometry analysis, cells were stained as described previously [28]. Briefly, cells were passed through a 40 µm cell strainer, washed with PBS, and incubated with the following antibodies: eFluor® 450- or APC-eFluor® 780-conjugated anti-CD45 (clone 30-F11, eBiosciences), APC-Cy7-conjugated anti-CD4 (clone GK1.5, BD Pharmingen™), PE- or PE-Cy7-conjugated anti-CD3e (clone 145-2C11, eBiosciences), PE-conjugated anti-Siglec-F (clone E50-2440, BD Pharmingen™), FITC- or BV421-conjugated anti-γδ T-Cell Receptor (clone GL3, BD Pharmingen™), FITC-conjugated anti-Vγ3 TCR (clone 536, BD Pharmingen™), FITC-conjugated anti-F4/80 (clone Cl:A3-1, Bio-Rad) or APC-Cy7-conjugated Ly-6G (clone E50-2440, BD Pharmingen™) in FACS buffer. Dead cells were excluded using 7-amino-actinomycin D (7-AAD) (BD Biosciences). Cells were analyzed on a FACSCanto II flow cytometer (BD), which was equipped with FACSDiva software (BD). For flow cytometry sorting, GFP^+ keratinocytes were sorted by FACSAria cell sorting system (BD).

RNA transcriptomics and GSEA

Total RNA was extracted from separated epidermal tissue using RNeasy Minikit (Qiagen) and RNA quality was determined using an Agilent 2200 TapeStation. Preparation of amplification reactions of complementary DNA (cDNA) was performed at the Cologne Center for Genomics (CCG) using Ovation RNA-Seq System V2 (NuGen) and library was prepared using the Nextera XT library preparation kit (Illumina). RNA sequencing was carried out on Illumina HiSeq2000 machines using the 2_100-bp protocol and V3 chemistry. After quality control, adapter sequences were removed by flexbar63. Reads mapping to ribosomal RNA-related genes were filtered out using a custom ribosomal RNA-only reference. After pre-processing, reads were mapped to the *Mus musculus* reference genome (build GRCm38_79), followed by differential gene expression analysis using the DESeq2 R library (version 1.6.3). Hierarchical clustering was performed in *R*. Transcripts regulated greater than 1.5 fold with a p value of < 0.05 were used in GO term analysis (DAVID Bioinformatics Resources 6.8) to identify enriched functional annotations. Gene set enrichment analysis was performed on whole gene list and compared to the Broad Institute Molecular Signatures Database collection of chemical and genetic perturbations (C2) using the Web-based tool available from the Broad Institute [29]. Enrichments with an FDR value < 0.05 were considered significant.

CE isolation for microscopy

A defined area of dorsal mouse skin (25 mm^2) was boiled in isolation buffer (20 mM Tris-HCl, pH 7.5, 5 mM EDTA, 10 mM DTT, and 2% SDS) under vigorous shaking for 40 min. After centrifugation, the CEs were washed twice with isolation buffer and were analyzed using a hemocytometer [30].

238

239 **Lipid analysis**

240 For the analysis of SC lipids, the SC was separated from the back skin of newborn mice
241 by floating the skin with the dermis side down on 0.5% trypsin in phosphate buffered
242 saline (PBS) for 24 h at 37 °C [31]. The SC was washed in PBS, lyophilized and weighed.
243 Lyophilized SC was homogenized in 0.5 ml of water using the Precellys 24
244 Homogenisator (Peqlab, Erlangen, Germany) at 6,500 rpm for 30 sec. After the addition
245 of 0.5 ml of water and 2 ml of chloroform/methanol 1:2 (v/v), freely extractable SC lipids
246 were extracted for 24 h at 37 °C and purified using a modification of the Bligh-Dyer
247 procedure as previously described [32]. For lipid quantification, the equivalent of 1.1 mg of
248 lyophilized SC was loaded on 20 × 10 cm HPTLC plates which were developed twice in
249 chloroform/methanol/glacial acetic acid 190:9:1 (v/v/v). Quantitative analytical TLC
250 determination was performed as previously described [33]. Nile red staining was performed
251 on cryo-sections for 2 min with 0.2 mg/ml Nile red in 75% glycerol; the fluorescence
252 intensity of Nile red stained epidermis was determined by integrated density using
253 ImageJ software.

254

255 **Trans-epidermal water loss (TEWL) measurements**

256 TEWL measurements were carried out as described previously [18] using a Tewameter
257 (Courage and Khazaka Electronic GmbH, Cologne, Germany) and the measurements
258 were performed according to the manufacturer's instructions.

259

260 **Irritant and allergic contact dermatitis**

To assess irritant contact dermatitis (ICD), the inner and outer surface of right ear was treated with 5 µl 1% croton oil in acetone/olive oil (4:1). The left ear was treated with acetone/olive oil only and taken as a control. Ear thickness was measured 4, 8, and 24 h after the treatment using a digital caliper. Ear swelling was determined by calculating the changes of ear thickness between challenged ear (right) and control ear (left). To evaluate hapten-induced allergic contact dermatitis (ACD), mice were sensitized by painting 25 µl of 1% 1-fluoro-2,4-dinitrobenzene (DNFB) (Sigma) in acetone/olive oil (4:1) onto the shaved abdominal skin at day 0. At day 6, mice were challenged by applying 5 µl 0.4% DNFB in acetone/olive oil on the inner and outer surface of right ear, respectively. The left ear was treated with acetone/olive oil only and taken as a control. Ear thickness was measured 8, 24, and 48 h after the treatment using a digital caliper. Ear swelling was determined by calculating the changes of ear thickness between challenged ear (right) and control ear (left).

Cell culture

Keratinocytes were isolated from newborns and cultured in low Ca^{2+} medium as described previously [27]. Briefly, skin was floated, dermal side down, on 0.25% trypsin solution (Gibco) for 16 h at 4°C. Epidermis was separated from the dermis and minced with a scalpel. Cell and epidermal tissue were suspended, shaken for 30 min at 37°C, and seeded on collagen-coated 6-well plates with mitomycin C- (Sigma) treated 3T3 fibroblast feeder layer cells. For the induction of keratinocyte differentiation, the medium was supplemented with 0.2 mM $CaCl_2$ (high Ca^{2+} medium).

Plasmids, virus preparation, and keratinocyte infection

MSCV-IRES-green fluorescent protein (GFP) retrovirus vector with myr-AKT was used as described previously [34]. myr-AKT-IRES-GFP and IRES-GFP retroviral supernatants were produced in 293T cells as previously described [35]. Briefly, 293T cells were transfected with vector constructs and packaging plasmids (pVPack-GP and pVPack-Eco; Stratagene). Forty-eight hours after transfection, virus supernatant was harvested and concentrated by precipitation with chondroitin 6-sulfate (CSC) (Sigma) and polybrene (Sigma), and centrifuged. Keratinocytes (P2) were exposed to concentrated viruses for 24 h and GPF^{+} cells were sorted by flow cytometry.

qRT-PCR analysis

RNA from epidermis and skin was extracted using an RNA isolation kit (Qiagen) according to the manufacturer's instructions. Reverse transcription of isolated RNA was performed using the High Capacity cDNA RT Kit (Applied Biosystems). Amplification reactions were performed with PowerSYBR Green PCR Master Mix (Applied Biosystems) using a 7300 Real Time PCRsystem (Applied Biosystems). The comparative method of relative quantification ($2^{-\Delta\Delta}$Ct) was used to calculate the expression level of the target gene normalized to GAPDH. Primer sequence information can be found in Supplemental Table 2.

Western blot analysis

Epidermis was separated from the dermis and dissociated with a MixerMill. For analysis of filaggrin, loricrin and keratin epidermis was lyzed in a 4% SDS lysis buffer.

Alternatively, cells or tissues were lyzed in radio immunoprecipitation assay (RIPA) buffer, containing protease inhibitor (Sigma-Aldrich) and phosphatase inhibitor (Roche). Protein concentration was determined by Micro BCA Protein Assay Kit (Thermo Scientific) and 20 mg protein per sample was subjected to SDS-PAGE (Invitrogen). Subsequently, protein was blotted to PVDF membranes. After blocking (5% non-fat milk in TBST buffer), membranes were incubated with primary antibodies. Antibody information can be found in Supplemental Table 1. For densitometry analysis, enhanced chemiluminescence exposed film was scanned and quantified with ImageJ software. Briefly, images were convered to grayscale and the background was removed. The densitometry was achieved by Gel Analysis method with ImageJ software. The ratio of filaggrin monomer and total filaggrin, pro-filaggrin and β-actin were determined with control set to 1 or the relative intensity was calculated after normalizing to a loading control (β-actin).

Statistical analysis.

Data are presented as mean ± s.e.m. and statistics was performed using PRISM software (GraphPad, version 5.0a). Statistical significance of difference was determined using unpaired 2-tailed Student's *t*-test or ANOVA one-way test analysis with Bonferroni multiple comparison test. *P* value <0.05 was considered to be statistically significant.

Journal Pre-proof

Results

Ric^{EKO} mice display a transient ichthyosis-like phenotype

To explore the role of epidermal mTORC2 signaling, we knocked out *Rictor* specifically in the epidermis as previously described [18]. Briefly, mice carrying a loxP-flanked *Rictor* allele were crossed with a transgenic mouse expressing Cre recombinase under the control of the human keratin 14 (K14) promoter [36-37], leading to epidermis-specific deletion of *Rictor* (Ric^{EKO}) in all basal cells and their progeny (Supplemental Figure 1A). Epidermis-specific Cre-mediated recombination of floxed *Rictor* alleles, verified by PCR analysis of genomic DNA extracted from different organs including the epidermis, resulted in effective epidermal loss of Rictor protein expression as confirmed by Western blot analysis and immunohistochemical staining (Figure 1A and Supplemental Figure 1B and C). Immediately after birth, Ric^{EKO} mice were clearly distinguishable from their wildtype littermates, exhibiting shiny, translucent and fragile skin. Occasionally, Ric^{EKO} newborns showed small erosions at the trunk, which might have occurred due to mechanical stress of the skin during birth. This skin fragility may have led to the observed death of approximately 20% of the mutant mice before or after weaning (Supplemental Figure 1D). By day 7 (P7), a prominent phenotype of dry and scaly, ichthyosis-like skin was apparent, often beginning with scaling of the ventral side already around P3 (Figure 1B). Histological analysis revealed a stratified epidermis but significantly reduced epidermal thickness in Ric^{EKO} pups at P4 (Figure 1C). Epidermal atrophy was primarily due to reduced granular cell layers and thinner SC. In addition, the SC in Ric^{EKO} mice displayed structural defects including poor organization of upper SC layers and densely packing of lower ones compared with the well-defined basket weave-

like structure in controls (Figure 1C). Although less pronounced, the epidermal atrophy remained detectable in adults (P70) (Supplemental Figure 1E). Morphological alterations in the epidermis of Ric^{EKO} newborns were paralleled by a transient impairment of epidermal barrier function as revealed by a significant increase in trans-epidermal water loss (TEWL) in P4 mutants (Figure 1D, Supplemental Figure 1F). As assessed by immunofluorescent staining for multiple tight/adherent junction proteins and components of desmosomal plaques, intercellular junctions appeared to be similar in control and Ric^{EKO} epidermis (Supplemental Figure 1G). Ric^{EKO} mice were born at the expected Mendelian ratio and exhibited normal body weight at birth, yet their weight by P5 decreased by 20% compared with littermate controls; the smaller body size persisted throughout adulthood (Figure 1E, Supplemental Figure 1H).

Ric^{EKO} mice display increased corneocyte fragility

To test whether epidermal atrophy and mechanical fragility in young Ric^{EKO} mice was associated with decreased physical resistance of the SC, cornified envelopes (CE) were prepared from the back skin of control and Ric^{EKO} mice at P5. Notably, 80% of CE isolated from control mice remained in a uniformly rigid, large and intact, polygonal shape, whereas more than 60% of Ric^{EKO} CE were ruptured, irregular, and fragmented, which is indicative of significant fragility and structural defects (Figure 1F).

Ultrastructural analysis of P5 epidermis by transmission electron microscopy (TEM) showed that the inner portion of Ric^{EKO} epidermis, including basement membrane, stratum basale and stratum spinosum, as well as desmosomal plaques were not grossly affected (Supplemental Figure 1I). However, detailed inspection revealed that keratin

intermediate filaments in the mutant mice were not condensed and were more loosely packed compared to controls (Figure 1G), which may contribute to the reduced resistance to mechanical stress in Ric^{EKO} CE. Together, our findings demonstrate major structural defects in the formation of the SG and SC in the absence of epidermal mTORC2 activity.

Epidermal mTORC2 deficiency induces a compensatory transcriptional epidermal repair program in Ric^{EKO} mice

To identify specific genes and pathways mediating mTORC2 signaling and orchestrating the SG to SC transition, we performed a RNA-sequencing (RNA-seq) transcriptome analysis of epidermis from mutant and control embryos at E19.5, when epidermal maturation nears completion and epidermal gene expression is not influenced by exposure to environmental insults that could mask primary mechanistic effects.

A one-way analysis of variance was performed to calculate the most variable and differentially expressed genes between both sets of epidermal tissue (fold change >2 and with P value < 0.05). Analysis revealed 231 and 249 genes down- and up-regulated, respectively, in Ric^{EKO} epidermis versus controls (Figure 2A). To identify biological processes underlying the observed gene expression alterations, we performed Gene Ontology Enrichment analysis (GO) and Pathway Enrichment analysis of the differentially expressed genes at the 1.5-fold cut-offs using DAVID 6.8. The upregulated gene set was particularly enriched in genes involved in peptide cross-linking (e.g. *Lce3a/b*, *Sprr1a*, and *Sprr2h*), keratinization (e.g. *Krt6a*, *Krt16*), keratinocyte differentiation (e.g. *Sfn*, *Sprr1a, Lce3a*), and wound repair (e.g. *Krt6a, Krt16, S100a8*) among others. The downregulated gene set was highly enriched for immune regulators

(e.g. *Oas1f*) and lipid metabolism (e.g. *Elovl3/4, Pnpla5, Pla2g5*) (FDR < 0.05) (Figure 2A and B). One of the most striking features of the RNA-seq data was the upregulation of genes for late keratinocyte differentiation and SC components, including small proline-rich proteins (Sprr), late cornified envelope proteins (Lce), and S100 proteins (Figure 2A). Several of these gene families comprise the epidermal differentiation complex (EDC), encoding a dense cluster of genes whose protein products have been identified as major molecular markers and important functional regulators for terminal differentiation in the stratified epidermis (Figure 2C) [38]. A panel of differentially regulated genes was confirmed by qRT-PCR-analysis, validating the RNA-seq data (Figure 2D). Further, gene set enrichment analysis (GSEA) revealed an upregulation of stress-response signatures in Ric^{EKO} epidermis compared to control, including epidermal barrier stress response regulators (e.g. *Krt6a, Krt16*) [39] and UVB-induced genes in human epidermis (e.g. *S100a8, Tnfrsf10b, Il24, Mmp3*) (Figure 2D and E) [40]. Collectively, these findings reveal profound alterations in mTORC2 deficient epidermis in gene regulatory networks controlling terminal differentiation and barrier formation, and implicate a critical role for mTORC2 activity in the formation of a protective epidermal barrier.

mTORC2 controls epidermal lipid metabolism

Keratinocytes of the granular layer contribute to epidermal lipid synthesis which is essential for effective skin barrier function [6, 41]. During cornification, lipids are packed in intracellular lamellar bodies (LB) which then transport and release the lipids into the intercellular space of corneocytes to form a lipid bilayer. The lipid bilayer mainly consists of ceramides, cholesterol, and FFA [6]. To examine whether the structural and

functional SC defects in Ric^{EKO} mice resulted from altered lipid composition, we further analyzed the SC lipid composition. Nile red, a fluorescent lipophilic dye, revealed that the lipid content was markedly diminished in Ric^{EKO} SC (Figure 3A). To quantify SC lipid composition, the levels of ceramides, cholesterol, and FFA in the SC were determined using high performance thin layer chromatography (HPTLC). The analysis revealed a decrease of all three main SC lipid classes in Ric^{EKO} epidermis. In particular, levels of Cer (NS) in Ric^{EKO} epidermis were decreased by more than 40% compared to controls (Figure 3B).

Notably, consistent with the reduced SC lipid composition, the GSEA of RNA-seq data revealed a panel of lipid metabolism-associated genes which were significantly downregulated in Ric^{EKO} epidermis. These genes include *Elovl3/4*, *Psap*, *Lipn*, *Pla2g3/5*, *Abhd5* (Figure 3C and D). Of note is that most of these genes have been shown to play a critical role in lipid metabolism and epidermal barrier formation in mice and patients with compromised skin barrier function [42].

At the interface between the SG and SC, lipid lamellae are released into the intercellular space. We further examined the organization of LB. In line with the altered epidermal lipid composition, ultrastructural analysis by TEM revealed impaired lipid lamellae structure in the LB of Ric^{EKO} epidermis. In addition, in Ric^{EKO} epidermis, the lipid layer between SC and the SG was disrupted (Figure 3E). Taken together, these findings reveal multiple quantitative defects in SG lipid synthesis that lead to altered lipid composition and LB structure in mTORC2-deficient epidermis, potentially contributing to the compromised epidermal barrier function in Ric^{EKO} mice.

Reduced proteolytic activity is paralleled by impaired filaggrin processing in mTORC2 deficient epidermis

Intriguingly, further pathway enrichment analysis using the KEGG database uncovered highly deregulated lysosomal transcripts in Ric^{EKO} epidermis (Figure 4A). Genetic skin diseases and conditions with disturbed barrier function are often characterized by a disturbed balance of epidermal protease and antiprotease activities [43]. We thus hypothesized that attenuated proteolytic activity in Ric^{EKO} epidermis might contribute to the disturbed barrier formation and function. Transcripts of several genes encoding members of diverse protease families, such as lysosomal cysteine, aspartic acid, and serine proteinases, were downregulated, including *cathepsin H* (*Ctsh*) and *cathepsin D* (*Ctsd*) (Figure 4B, C). Of interest is that *CTSH* and *CTSD* mutations have recently been shown to cause impaired filaggrin processing and disturbed SC formation [26, 44]. Conversely, Serpins, which encode potent protease inhibitors, were upregulated, including *Serpinb2*, which encodes an ovalbumin-like serine protease inhibitor and has been linked to the pathogenesis of certain cornification disorders [45] (Figure 4B, C). Moreover, expression of the gene encoding secretory leukocyte peptidase inhibitor (*Slpi*) was markedly increased in Ric^{EKO} epidermis (Figure 4D). *Slpi* encodes an inhibitor of kallikrein 7, a protease required for corneodesmosome cleavage. Interestingly, TEM revealed that corneodesmosomes were retained in Ric^{EKO} epidermis with an increase in both number and size (Figure 4E), thereby further corroborating an attenuated corneodesmosome degradation in the Ric^{EKO} SC, potentially due to reduced Slpi.

Further, proteolytic processing of the CE reinforcement protein profilaggrin is an essential process during proper keratinocyte terminal differentiation [9]. Having found that

Ctsh and *Ctsd*, encoding two proteases critically involved in profilaggrin processing, are downregulated in Ric^{EKO} epidermis, we analyzed profilaggrin protein expression and processing in extracts prepared from control and Ric^{EKO} epidermis by Western blot analysis. Notably, while filaggrin mRNA and profilaggrin protein expression levels were comparable between control and Ric^{EKO} epidermis at P5, the level of filaggrin monomer was markedly reduced in mutant epidermis, suggesting that decreased epidermal protease activity might affect filaggrin processing in Ric^{EKO} epidermis (Figure 4F and 4G).

A keratinocyte-autonomous mTORC2-Akt axis controls filaggrin processing

To tackle the molecular mechanism underlying decreased filaggrin processing in Ric^{EKO} epidermis, we isolated primary keratinocytes from control and Ric^{EKO} newborn mice and analyzed downstream targets of mTOR pathways during terminal differentiation triggered by Ca^{2+} treatment [46-47]. Ca^{2+} triggered activation of both mTORC1 (pS6-Ser240/244) and mTORC2 (pAkt-Ser473) in wild-type keratinocytes (Figure 5A). As expected, the absence of mTORC2 in Ric^{EKO} keratinocytes abolished phosphorylation of Akt-Ser473 in response to Ca^{2+} exposure (Figure 5A). Earlier studies had demonstrated that Akt is a critical regulator of profilaggrin processing during keratinocyte differentiation [24-25]. Notably, Western blot analysis revealed a pronounced reduction of processed trimer and monomer filaggrin in Ric^{EKO} keratinocytes. Signals for other markers of keratinocyte differentiation, including loricrin and keratin 10 (K10), appeared unchanged in the knockout mice (Figure 5B).

To better define the role of mTORC2-mediated filaggrin processing, we retrovirally reconstituted Ric^{EKO} keratinocytes with constitutively active myristoylated Akt1 (myr-

AKT) [34] and examined filaggrin processing. Empty pMSCV-IRES-GFP vector transfection served as control. Infection efficiencies were determined by analysis of IRES-driven GFP expression. GFP^+ cells were sorted by flow cytometry (FACS), expanded *in vitro*, and subjected to high Ca^{2+}-induced differentiation. Western blot analysis confirmed abundant myr-AKT protein expression and increased Akt-Ser473 phosphorylation signal in myr-AKT transduced keratinocytes (Figure 5C and D). In line with previous studies[24-25], enforced myr-Akt expression increased filaggrin monomer expression in control keratinocytes upon calcium-triggered differentiation (Figure 5C). Importantly, restoration of Akt signaling in Ric^{EKO} keratinocytes resulted in a significant increase in the amount of filaggrin monomer (Figure 5D), indicating that restored Akt-Ser473 phosphorylation enhanced filaggrin processing in Ric^{EKO} cells. Taken together, our findings implicate mTORC2-mediated activation of Akt-Ser473 as a critical factor in effective filaggrin processing in keratinocyte terminal differentiation.

Epidermal mTORC2 determines immune cell composition in the skin

Epidermal barrier defects are often associated with altered immune responses and inflammatory skin diseases [48]. To assess the consequences of epidermal mTORC2-deficiency and the resulting barrier defect on the immune status, we examined inflammation mediator expression in prenatal E19.5 epidermis (RNA-seq analysis) and in P5 Ric^{EKO} epidermis by qRT-PCR. Notably, whereas the RNA-seq analysis in prenatal E19.5 epidermis revealed downregulation of inflammation mediators when compared to controls (Figure 2B; Supplemental Table 3), postnatal (P5) expression of thymic stromal lymphopoietin (*Tslp*) and interleukin-24 (*Il24*) were markedly increased in Ric^{EKO}

epidermis compared to littermate controls (Figure 6A). In contrast, transcripts for other potent inflammatory factors, including interleukin-1α (*Il1α*), interleukin-1β (*Il1β*), interleukin-33 (*Il33*), chemokine ligand (*Ccl2*), and tumor necrosis factor-α (*Tnfα),* were not obviously altered in P5 Ric^{EKO} epidermis (Figure 6A). To investigate further the impact of epidermal mTORC2 activity on cutaneous immune cell composition, we also performed immunohistochemical and fluorescent analyses in back skin of controls and Ric^{EKO} mice at P5. While no major difference was detected in numbers of toluidine blue stained mast cells and dermal $F4/80^+$ macrophages, the number of dermal $CD4^+$ T cells was increased in Ric^{EKO} mice (Figure 6B; Supplemental Figure 2A). The tendency towards an increase in $CD4^+$ cells in Ric^{EKO} skin was corroborated by FACS analysis. Unexpectedly, these analyses further revealed that the percentage of $CD3^+$γδ-TCR^+ cells (Gate: 7-AAD^-CD45^+) was markedly reduced from 5.314±0.708% to 0.350±0.085% in Ric^{EKO} skin (Figure 6C; Supplemental Figure 2B).

Dendritic epidermal T cells (DETCs) constitute a subset of T cells, which highly express the γδ-T cell receptor (γδ-TCR) and specifically localize to the epidermis [49-50]. Consistent with the FACS analysis, immunofluorescent staining for the pan-T cell marker CD3 revealed a pronounced reduction of epidermal T cells in Ric^{EKO} mice as compared to controls (Figure 7A). Further, epidermal CD3 and γδ-TCR co-staining revealed significantly reduced DETCs in Ric^{EKO} epidermis (Figure 7A). Intriguingly, RNA-seq analysis of E19.5 Ric^{EKO} epidermis revealed a significant downregulation of several members of the *Skint* family genes when compared to controls (Figure 7B). γδ-TCR ligand *Skint* genes are expressed by epidermal keratinocyte and play a critical role in maintaining the DETC pool in the epidermis and in regulating γδ-TCR cell homeostasis

534 [51]. Downregulated expression of *Skint1* and *Skint4* was confirmed by qRT-PCR analysis
535 in control und mutant epidermis at P0 (Figure 7C).
536 To answer the question whether epidermal mTORC2 activity is important to maintain the
537 homeostasis of DETCs throughout adulthood, we analyzed whole mounts from ear skin
538 in adult mice at P70. Immunofluorescent analysis and FACS analysis revealed that the
539 number of $CD45^+CD3e^+\gamma\delta\text{-}TCR^{high}V\gamma3^+$ DETCs was also markedly reduced in adult
540 Ric^{EKO} epidermal sheets, whereas the proportion of $CD45^+CD3e^+\gamma\delta\text{-}TCR^{low}V\gamma3^-$ dermal
541 γδ T cells was similar in Ric^{EKO} mice and controls (Figure 7D, E; Supplemental Figure
542 2C). Interestingly, the majority of DETCs in Ric^{EKO} ears displayed an activated
543 phenotype characterized by a rounded morphology and reduced dendritic spines as
544 compared to DETCs in controls (Figure 7D). Reduced DETC number was paralleled by
545 significantly reduced *Skint1* and *Skint4 transcripts* (Figure 7F). Collectively, these
546 findings reveal a critical role of epidermal mTORC2 activity in determining the
547 composition of T cell subpopulations in naïve skin.
548
549 **DNFB-mediated percutaneous immune response is enhanced in Ric^{EKO} mice**
550 Barrier disruption and continuous percutaneous exposure to allergens presumably initiate
551 and drive a variety of inflammatory skin diseases, including AD [52]. In fact, long-term
552 observation under specific pathogen free (SPF) conditions revealed mildly dry eyes and
553 perioral dermatitis in Ric^{EKO} mice, to varying extent among individual mutants
554 (Supplemental Figure 3A). Numbers of mast cells, $CD4^+$ T cells, and $F4/80^+$ myeloid
555 cells and transcripts of proinflammatory mediators including *Il6, Tnfα, Il1β,* and *Tslp*
556 showed a tendency towards increase, yet, the difference did not reach statistical

557 significantly in unchallenged back skin of control and mutants at 10 weeks (Supplemental
558 Figure 3B and C). In addition, although serum levels of circulating total IgE were
559 increased in Ric^{EKO} mice at 10 weeks, the difference did not reach statistical significance
560 (Supplemental Figure 3D). To quantify the functional impact of epidermal mTORC2
561 activity in percutaneous immune responses to exogenous substances, 10 week-old control
562 and Ric^{EKO} mice were subjected to established models of irritant (ICD) or allergic (ACD)
563 contact dermatitis. Whereas no difference in ICD was observed between control and
564 mutants (Supplemental Figure 3E), ACD in response to the hapten DNFB was
565 significantly pronounced in mutants versus controls (Figure 8A). In controls the positive
566 DNFB response was paralleled by a significant increase in epidermal phosphorylation of
567 Akt-S473, an alteration of the cellular immune cell infiltrate with significant increase in
568 numbers of $F4/80^+$ myeloid cells and a significant decline in DETCs (Figure 8C and
569 Supplemental Figure 4). In contrast, the attenuated DNFB response in Ric^{EKO} epidermis
570 was associated with a significant reduction of epidermal Akt-S473 phosphorylation, an
571 alteration of the cellular immune cell infiltrate with significant increase in numbers of
572 granulocytes, $F4/80^+$ myeloid and $CD4^+$ T cells, and virtually absence of DETCs;
573 differences in $F4/80^+$ myeloid cell, $CD4^+$ T cell and DETC cell infiltrate were
574 significantly different in Ric^{EKO} versus control mice (Figure 8C and Supplemental Figure
575 4). In addition, transcripts of stress response genes including *Krt6b*, *S100a8* and *Sprr2d*,
576 and proinflammatory mediators such as *Il6*, *Tnfα* and *Il24*, were significantly increased in
577 DNFB challenged ear skin in Ric^{EKO} versus controls (Supplemental Figure 5).

578 Taken together, these findings strongly suggest that the impaired epidermal barrier in
579 Ric^{EKO} mice allows an increased hapten penetration, which in turn leads to the
580 exaggerated stress and percutaneous immune responses.
581

Journal Pre-proof

Discussion

In the present study, we describe epidermal mTORC2 as central hub orchestrating the complex multicellular crosstalk and signaling required for postnatal epidermal barrier integrity and function. Specifically, we uncover a key role for epidermal mTORC2 activity in the assembly of a protective SC (Figure 8D).

A prominent phenotype of Ric^{EKO} mice is the dry, scaly, and ichthyosis-like appearance of skin. A similar phenotype is present in various mouse mutants and human skin diseases with epidermal barrier defects including ichthyosis, AD and multiple clinical eczema variants [16, 53]. Yet, an overarching mechanism that controls the multiple molecular factors in epidermal barrier formation is not resolved. Here, we propose the Ric^{EKO} mouse as a novel preclinical disease model to advance our incomplete understanding of the molecular regulation of SC assembly and epidermal barrier function. Ric^{EKO} mice displayed multiple skin symptoms which are also hallmarks in patients with compromised epidermal barrier function, including increased SC fragility and increased TEWL [6]. Ric^{EKO} epidermis also showed dysbalanced protease/antiprotease activities combined with attenuated filaggrin processing, both previously reported to be associated with skin barrier defects in patients [26, 44, 54-55]. Thus, here we identified mTORC2 as a critical regulator of protease-mediated epidermal terminal differentiation.

In addition, a striking feature of *Rictor*-deficient epidermis is disturbed lipid composition. Specifically, we observed quantitative alterations in lipid content and structural alterations in lipid lamellae formation in Ric^{EKO} epidermis. Consistently, expression of multiple genes previously reported to be essential in epidermal lipid synthesis and epidermal function in humans were reduced in Ric^{EKO} epidermis emphasizing the utility

of Ric^{EKO} mice as an attractive preclinical disease model for barrier defects [10, 12-15]. Recent reports describing a regulatory role for mTORC2 in *de novo* lipid synthesis are limited to hepatic and adipose tissues [56-58]. Here, we provide the first evidence of a role for mTORC2 in epidermal lipid metabolism. However, although it is widely accepted that epidermal lipids are integral components driving the formation and maintenance of the epidermal permeability barrier, the exact mechanistic link how epidermal lipids regulate epidermal barrier function and/or vice versa, is not entirely resolved [59,60]. Therefore, although our findings in Ric^{EKO} mice suggest that the quantitative and qualitative perturbations in lipid composition is causative for the observed skin barrier defect in Ric^{EKO} mice, at this stage we cannot exclude the possibility that perturbed epidermal architecture contributes to perturbed lipid synthesis [59, 60]. It will be of interest to investigate in future studies additional downstream mediators of mTORC2 signaling to understand how epidermal *de novo* lipogenesis and SC lipid homeostasis is regulated by mTORC2.

Intriguingly, the number of epidermal DETCs was remarkably reduced in Ric^{EKO} mice. DETCs are profoundly reduced in patients with AD as well as in mouse models lacking key SC proteins [30,61]. Consistent with a reduced DETC number in Ric^{EKO} epidermis, the expression of several members of *Skint* family genes was downregulated in Rictor-deficient epidermis. *Skint* genes have been identified as essential regulators of DETC cell development [50]. Hence, our findings indicate that epidermal mTORC2 activity is critical for anchoring DETCs in the epithelial niche and maintaining the DETC repertoire, potentially mediated via *Skint* genes. However, the reduced epidermal DETC number could be caused by a combination of multiple factors including attenuated expression of

628 *Skint* genes, perturbed epidermal architecture and/or disturbed interplay between lipids
629 and/or additional factors and remains to be further investigated in future studies. In
630 addition to the reduced number of epidermal DETCs, the morphology of DETCs was
631 significantly altered in Ric^{EKO} epidermis. DETCs in Ric^{EKO} epidermal sheets lead to a
632 phenotype associated with activation and a protective role in injured epidermis [50]. Thus, it
633 is tempting to speculate that DETCs in Ric^{EKO} epidermis compensate for a defective
634 epidermal barrier. Together, our findings suggest an important function of epidermal
635 mTORC2 in maintaining and shaping DETC homeostasis, and thus, highlight a
636 previously unrecognized function of mTORC2 in the epithelial-immune crosstalk
637 regulating skin barrier function. Along these lines, increased infiltration of $CD4^+$ T cells
638 and enhanced expression of *Tslp* were also observed in the skin of Ric^{EKO} pups, both of
639 which are hallmarks in epidermis and keratinocytes of AD patients [62]. Although, the adult
640 Ric^{EKO} mouse skin displayed no spontaneous pathological phenotypes, including skin
641 lesions or signs of skin inflammation, adult mutants exhibited exaggerated percutaneous
642 immune responses. AD patients have an increased risk of sensitization to allergens, as
643 well as asthma, rhinitis, and food allergy. Consistently, *FLG* deficiency in mice facilitates
644 and permits increased percutaneous sensitization with protein allergens, irritants, and
645 haptens [63-64]. Collectively, our findings highlight a direct link between epidermal
646 mTORC2 deficiency and paradigmatic symptoms of patients with defective epidermal
647 barrier conditions such as ichthyosis or AD.
648 An important question is what could be the mechanistic explanation for the various
649 processes and symptoms observed in Ric^{EKO} mice? A well-defined function of mTORC2
650 is the phosphorylation of Akt at Ser473, which contributes to Akt-Thr308

651 phosphorylation by the phosphoinositide-dependent kinase 1 (PDK1), leading to full Akt
652 activation [20, 65]. Akt activity is elevated at the onset of keratinocyte differentiation and has
653 been shown to regulate epidermal terminal differentiation [18,24-25]. However, the signaling
654 events triggering epidermal Akt activation in epidermal differentiation still remain
655 elusive. We propose a non-redundant role for mTORC2 in Akt-Ser473 activation during
656 epidermal stratification and cornification. It is likely that epidermal mTORC2 acts
657 through Akt in a PDK1-dependent manner since depletion of either component leads to
658 an epidermal barrier phenotype comparable to that in Ric^{EKO} mice [66-67]. Several *in vitro*
659 and *in vivo* studies suggest that proper filaggrin processing requires Akt activation [24-26].
660 Accordingly, we observed that Akt-Ser473 phosphorylation was significantly attenuated
661 and filaggrin processing was impaired in Ric^{EKO} keratinocytes *in vitro*. Together, our
662 findings suggest that the mTORC2-Akt signaling axis is activated and has mTORC1-
663 independent functions upon terminal differentiation to trigger filaggrin processing and
664 barrier function. Future studies are needed to determine whether induction of epidermal
665 protease activity and/or lipid metabolism is a direct or indirect downstream target of
666 mTORC2-Akt signaling.
667 Finally, prenatal Ric^{EKO} epidermis presented a robust upregulation of a stress-response
668 signature characterized by prominent expression of epidermal barrier stress-induced
669 intermediate filament genes as well as UVB-induced genes. We hypothesize that this
670 induced stress response supports a compensatory, protective mechanism in response to
671 the barrier defect, thereby ensuring survival. This hypothesis is further based on the
672 finding that the cytoprotective transcription factor *Nrf2* and several well known Nrf2-
673 target genes, including *Krt6, Krt16, Sprr2h,* and *S100a* were all transcriptionally

upregulated in Ric^{EKO} epidermis [68]. Along these lines, a Nrf2-regulated compensatory response has been shown to be activated in embryonic epidermis lacking loricrin [69]. Therefore, our findings support the idea that the activation of a stress-related homeostatis program is a general feature of a functionally compromised epidermal barrier. Our discovery that the druggable mTORC2 complex orchestrates this generalized stress response opens interesting avenues for exploring therapeutic boosting of barrier function.

In conclusion, we have demonstrated that postnatal epidermal mTORC2 activity orchestrates epidermal barrier formation and maintenance via regulation of lipid synthesis and filaggrin processing. We speculate that altered mTORC2 activity may represent another predisposing factor for skin disorders associated with disrupted barrier function. Our findings might be of clinical relevance by, for example, normalizing epidermal mTORC2 activity in patients with defective epidermal barrier conditions by pharmacotherapy.

Journal Pre-proof

Author Contributions

XD and SAE conceptualized the study, performed experiments, analyzed the data, and drafted the manuscript; WB performed TEM analysis; SW helped with flow cytometry and experimental animal work; PW performed the bio-informatic analyses; SB performed the lipid analysis; MNH and MAR provided *Rictor* floxed mouse lines; AJ, JCB, SAW, AR, MNH, MAR have made substantial contributions to the analysis and interpretation of data and critical revising of the drafted manuscript.

Acknowledgments

We thank Michael Piekarek, Gabriele Scherr, and Sebastian Wüst for excellent technical assistance. The authors thank Dr. Stephen M. Sykes (Fox Chase Cancer Center, Philadelphia) and Dr. Kira Gritsman (Department of Medicine, Albert Einstein College of Medicine) for the gift of the myr-AKT plasmid used in this study; we thank Dr. Sandra Iden for providing antibodies. We thank Dr. Carien Niessen and colleagues in her group for insightful suggestions and technical advice in TEWL measurements. We thank Dr. Peter Nürnberg and Dr. Janine Altmüller (Cologne Center for Genomics, University of Cologne, Germany) for supporting transcriptome and bioinformatic analyses. We also thank the Imaging Facility (CECAD, Cologne University) and Dr. Gunter Rappl, (Central Cell Sorting Facility, CMMC, Cologne University) for specialized technical support. The funding source for this manuscript was the Deutsche Forschungsgemeinschaft (SAE, SAW, JCB to Projektnummer 73111208 - SFB829 and CECAD), (SAE, AR to FOR2599), and the Center for Molecular Medicine (SAE).

References

1. Elias PM. Skin barrier function. Curr Allergy and Asthma Rep 2008; 8:299-305.
2. Kubo A, Nagao K, Amagai M. Epidermal barrier dysfunction and cutaneous sensitization in atopic diseases. J Clin Invest 2012; 122:440-447.
3. Duff M, Demidova O, Blackburn S, Shubrook J. Cutaneous manifestations of diabetes mellitus. Clin Diabetes 2015; 33:40-48.
4. Boireau-Adamezyk E, Baillet-Guffroy A, Stamatas GN. Age-dependent changes in stratum corneum barrier function. Skin Res Technol 2014; 20:409-415.
5. Craiglow BG. Ichthyosis in the newborn. Semin in Perinatol 2013; 37:26-31.
6. Candi E, Schmidt R, Melino G. The cornified envelope: a model of cell death in the skin. Nat Rev Mol Cell Biol 2005; 6:328-340.
7. Lopez-Pajares V, Yan K, Zarnegar BJ, Jameson KL, Khavari PA. Genetic pathways in disorders of epidermal differentiation. Trends Genet 2013; 29:31-40.
8. Smith FJD, Irvine AD, Terron-Kwiatkowski A, Sandilands A, Campbell LE, Zhao YW, et al. Loss-of-function mutations in the gene encoding filaggrin cause ichthyosis vulgaris. Nat Genet 2006; 38:337-342.
9. Sandilands A, Sutherland C, Irvine AD, McLean WH. Filaggrin in the frontline: role in skin barrier function and disease. J Cell Sci 2009; 122:1285-1294.
10. Brunner PM, Israel A, Zhang N, Leonard A, Wen HC, Huynh T, et al. Early-onset pediatric atopic dermatitis is characterized by T(H)2/T(H)17/T(H)22-centered inflammation and lipid alterations. J Allergy Clin Immunol 2018; 141:2094-2106.

11. Gruber R, Elias PM, Crumrine D, Lin TK, Brandner JM, Hachem JP, et al. Filaggrin Genotype in Ichthyosis Vulgaris Predicts Abnormalities in Epidermal Structure and Function. Am J Pathol 2011; 178:2252-2263.

12. Vasireddy V, Uchida Y, Salem N, Kim SY, Mandal MNA, Reddy GB, et al. Loss of functional ELOVL4 depletes very long-chain fatty acids (>= C28) and the unique omega-O-acylceramides in skin leading to neonatal death. Hum Mol Genet 2007; 16:471-482.

13. Westerberg R, Tvrdik P, Unden AB, Mansson JE, Norlen L, Jakobsson A, et al. Role for ELOVL3 and fatty acid chain length in development of hair and skin function. J Biol Chem 2004; 279:5621-5629.

14. Aldahmesh MA, Mohamed JY, Alkuraya HS, Verma IC, Puri RD, Alaiya AA, et al. Recessive mutations in ELOVL4 cause ichthyosis, intellectual disability, and spastic quadriplegia. Am J Hum Genet 2011; 89:745-750.

15. Ilic D, Bollinger JM, Gelb M, Mauro TM. sPLA2 and the epidermal barrier. Biochim Biophys Acta 2014; 1841:416-421.

16. Natsuga K. Epidermal Barriers. Cold Spring Harb Perspect Med 2014; 4:a018218.

17. Blanpain C, Fuchs E. Epidermal homeostasis: a balancing act of stem cells in the skin. Nat Rev Mol Cell Biol 2009; 10:207-217.

18. Ding X, Bloch W, Iden S, Ruegg MA, Hall MN, Leptin M, et al. mTORC1 and mTORC2 regulate skin morphogenesis and epidermal barrier formation. Nat Commun 2016; 7:13226.

Journal Pre-proof

19. Kakanj P, Moussian B, Gronke S, Bustos V, Eming SA, Partridge L, et al. Insulin and TOR signal in parallel through FOXO and S6K to promote epithelial wound healing. Nat Commun 2016; 7:12972.

20. Saxton RA, Sabatini DM. mTOR Signaling in Growth, Metabolism, and Disease. Cell 2017; 168:960-976.

21. Wullschleger S, Loewith R, Hall MN. TOR signaling in growth and metabolism. Cell 2006; 124:471-484.

22. Sarbassov DD, Ali SM, Sengupta S, Sheen JH, Hsu PP, Bagley AF, et al. Prolonged rapamycin treatment inhibits mTORC2 assembly and Akt/PKB. Mol Cell 2006; 22:159-168.

23. Jacinto E, Loewith R, Schmidt A, Lin S, Ruegg MA, Hall A, et al. Mammalian TOR complex 2 controls the actin cytoskeleton and is rapamycin insensitive. Nat Cell Biol 2004; 6:1122-1128.

24. Calautti E, Li J, Saoncella S, Brissette JL, Goetinck PF. Phosphoinositide 3-kinase signaling to Akt promotes keratinocyte differentiation versus death. J Biol Chem 2005; 280:32856-32865.

25. O'Shaughnessy RF, Welti JC, Cooke JC, Avilion AA, Monks B, Birnbaum MJ, et al. AKT-dependent HspB1 (Hsp27) activity in epidermal differentiation. J Biol Chem 2007; 282:17297-17305.

26. Naeem AS, Tommasi C, Cole C, Brown SJ, Zhu Y, Way B, et al. A mechanistic target of rapamycin complex 1/2 (mTORC1)/V-Akt murine thymoma viral oncogene homolog 1 (AKT1)/cathepsin H axis controls filaggrin expression and

775 processing in skin, a novel mechanism for skin barrier disruption in patients with
776 atopic dermatitis. J Allergy Clin Immunol 2016; 139:1228-1241.
777 27. Ding X, Lucas T, Marcuzzi GP, Pfister H, Eming SA. Distinct functions of
778 epidermal and myeloid-derived VEGF-A in skin tumorigenesis mediated by
779 HPV8. Cancer Res 2015; 75:330-343.
780 28. Knipper JA, Willenborg S, Brinckmann J, Bloch W, Maass T, Wagener R, et al.
781 Interleukin-4 Receptor alpha Signaling in Myeloid Cells Controls Collagen Fibril
782 Assembly in Skin Repair. Immunity 2015; 43:803-816.
783 29. Subramanian A, Tamayo P, Mootha VK, Mukherjee S, Ebert BL, Gillette MA, et
784 al. Gene set enrichment analysis: a knowledge-based approach for interpreting
785 genome-wide expression profiles. Proc Natl Acad Sci U S A 2005; 102:15545-
786 15550.
787 30. Sevilla LM, Nachat R, Groot KR, Klement JF, Uitto J, Djian P, et al. Mice
788 deficient in involucrin, envoplakin, and periplakin have a defective epidermal
789 barrier. J Cell Biol 2007; 179:1599-1612.
790 31. Reichelt J, Breiden B, Sandhoff K, Magin TM. Loss of keratin 10 is accompanied
791 by increased sebocyte proliferation and differentiation. Eur J Cell Biol 2004;
792 83:747-759.
793 32. Signorelli P, Hannun YA. Analysis and quantitation of ceramide. Methods
794 Enzymol 2002; 345:275-294.
795 33. Belgardt BF, Mauer J, Wunderlich FT, Ernst MB, Pal M, Spohn G, et al.
796 Hypothalamic and pituitary c-Jun N-terminal kinase 1 signaling coordinately
797 regulates glucose metabolism. Proc Natl Acad Sci U S A 2010; 107:6028-6033.

34. Kharas MG, Okabe R, Ganis JJ, Gozo M, Khandan T, Paktinat M, et al. Constitutively active AKT depletes hematopoietic stem cells and induces leukemia in mice. Blood 2010; 115:1406-1415.

35. Ding X, Wang X, Sontag S, Qin J, Wanek P, Lin Q, et al. The polycomb protein Ezh2 impacts on induced pluripotent stem cell generation. Stem Cells Dev 2014; 23:931-940.

36. Bentzinger CF, Romanino K, Cloetta D, Lin S, Mascarenhas JB, Oliveri F, et al. Skeletal Muscle-Specific Ablation of raptor, but Not of rictor, Causes Metabolic Changes and Results in Muscle Dystrophy. Cell Metab 2008; 8:411-424.

37. Hafner M, Wenk J, Nenci A, Pasparakis M, Scharffetter-Kochanek K, Smyth N, et al. Keratin 14 Cre transgenic mice authenticate keratin 14 as an oocyte-expressed protein. Genesis 2004; 38:176-181.

38. Mischke D, Korge BP, Marenholz I, Volz A, Ziegler A. Genes encoding structural proteins of epidermal cornification and S100 calcium-binding proteins form a gene complex ("epidermal differentiation complex") on human chromosome 1q21. J Invest Dermatol 1996; 106:989-992.

39. Lessard JC, Pina-Paz S, Rotty JD, Hickerson RP, Kaspar RL, Balmain A, et al. Keratin 16 regulates innate immunity in response to epidermal barrier breach. Proc Natl Acad Sci U S A 2013; 110:19537-19542.

40. Enk CD, Jacob-Hirsch J, Gal H, Verbovetski I, Amariglio N, Mevorach D, et al. The UVB-induced gene expression profile of human epidermis in vivo is different from that of cultured keratinocytes. Oncogene 2006; 25:2601-2614.

41. Elias PM, Williams ML, Holleran WM, Jiang YJ, Schmuth M. Pathogenesis of permeability barrier abnormalities in the ichthyoses: inherited disorders of lipid metabolism. J Lipid Res 2008; 49:697-714.

42. Breiden B, Sandhoff K. The role of sphingolipid metabolism in cutaneous permeability barrier formation. Biochim Biophys Acta 2014; 1841:441-452.

43. Ovaere P, Lippens S, Vandenabeele P, Declercq W. The emerging roles of serine protease cascades in the epidermis. Trends Biochem Sci 2009; 34:453-463.

44. Egberts F, Heinrich M, Jensen JM, Winoto-Morbach S, Pfeiffer S, Wickel M, et al. Cathepsin D is involved in the regulation of transglutaminase 1 and epidermal differentiation. J Cell Sci 2004; 117:2295-2307.

45. Oji V, Oji ME, Adamini N, Walker T, Aufenvenne K, Raghunath M, et al. Plasminogen activator inhibitor-2 is expressed in different types of congenital ichthyosis: in vivo evidence for its cross-linking into the cornified cell envelope by transglutaminase-1. Br J Dermatol 2006; 154:860-867.

46. Yuspa SH, Kilkenny AE, Steinert PM, Roop DR. Expression of murine epidermal differentiation markers is tightly regulated by restricted extracellular calcium concentrations in vitro. J Cell Biol 1989; 109:1207-1217.

47. Tu CL, Crumrine DA, Man MQ, Chang WH, Elalieh H, You M, et al. Ablation of the Calcium-Sensing Receptor in Keratinocytes Impairs Epidermal Differentiation and Barrier Function. J Invest Dermatol 2012; 132:2350-2359.

48. Elias PM. Therapeutic Implications of a Barrier-based Pathogenesis of Atopic Dermatitis. Ann Dermatol 2010; 22:245-254.

Journal Pre-proof

49. Komori H, Meehar TF, Havran WL. Epithelial and mucosal gamma delta T cells. Curr Opin in Immunol 2006; 18:534-538.

50. Nielsen MM, Witherden DA, Havran WL. γδ T cells in homeostasis and host defence of epithelial barrier tissues. Nat Rev Immunol 2017; 17:733-745.

51. Barbee SD, Woodward MJ, Turchinovich G, Mention JJ, Lewis JM, Boyden LM, et al. Skint-1 is a highly specific, unique selecting component for epidermal T cells. Proc Natl Acad Sci U S A 2011; 108:3330-3335.

52. De Benedetto A, Kubo A, Beck LA. Skin barrier disruption: a requirement for allergen sensitization? J Invest Dermatol 2012; 132:949-963.

53. Weidinger S, Novak N. Atopic dermatitis. Lancet 2016; 387:1109–22.

54. Toomes C, James J, Wood AJ, Wu CL, McCormick D, Lench N, et al. Loss-of-function mutations in the cathepsin C gene result in periodontal disease and palmoplantar keratosis. Nat Genet 1999; 23:421-424.

55. Cheng T, Hitomi K, van Vlijmen-Willems IMJJ, de Jongh GJ, Yamamoto K, Nishi K, et al. Cystatin M/E is a high affinity inhibitor of cathepsin V and cathepsin L by a reactive site that is distinct from the legumain-binding site - A novel clue for the role of cystatin M/E in epidermal cornification. J Biol Chem 2006; 281:15893-15899.

56. Caron A, Richard D, Laplante M. The Roles of mTOR Complexes in Lipid Metabolism. Annu Rev Nutr 2015; 35:321-348.

57. Guri Y, Colombi M, Dazert E, Hindupur SK, Roszik J, Moes S, et al. mTORC2 Promotes Tumorigenesis via Lipid Synthesis. Cancer Cell 2017; 32:807-823.

58. Hagiwara A, Cornu M, Cybulski N, Polak P, Betz C, Trapani F, et al. Hepatic mTORC2 Activates Glycolysis and Lipogenesis through Akt, Glucokinase, and SREBP1c. Cell Metab 2012; 15:725-738.

59. van Smeden J, Janssens M, Gooris GS, Bouwstra JA. The important role of stratum corneum lipids for the cutaneous barrier function. Biochim Biophys Acta 2014; 1841:295-313.

60. Bhattacharya N, Sato WJ, Kelly A, Ganguli-Indra G, Indra AK. Epidermal lipids: key mediators of atopic dermatitis pathogenesis. Trends Mol Med doi: 10.1016/j.molmed.2019.04.001 [Epub ahead of print May 01, 2019].

61. Katsuta M, Takigawa Y, Kimishima M, Inaoka M, Takahashi R, Shiohara T. NK cells and gamma delta(+) T cells are phenotypically and functionally defective due to preferential apoptosis in patients with atopic dermatitis. J Immunol 2006; 176:7736-7744.

62. Ziegler SF, Artis D. Sensing the outside world: TSLP regulates barrier immunity. Nat Immunol 2010; 11:289-293.

63. Kawasaki H, Nagao K, Kubo A, Hata T, Shimizu A, Mizuno H, et al. Altered stratum corneum barrier and enhanced percutaneous immune responses in filaggrin-null mice. J Allergy Clin Immunol 2012; 129:1538-1546.

64. Fallon PG, Sasaki T, Sandilands A, Campbell LE, Saunders SP, Mangan NE, et al. A homozygous frameshift mutation in the mouse Flg gene facilitates enhanced percutaneous allergen priming. Nat Genet 2009; 41:602-608.

65. Sarbassov DD, Guertin DA, Ali SM, Sabatini DM. Phosphorylation and regulation of Akt/PKB by the rictor-mTOR complex. Science 2005; 307:1098-1101.

66. Dainichi T, Hayden MS, Park SG, Oh H, Seeley JJ, Grinberg-Bleyer Y, et al. PDK1 Is a Regulator of Epidermal Differentiation that Activates and Organizes Asymmetric Cell Division. Cell Rep 2016; 15:1615-1623.

67. Peng XD, Xu PZ, Chen ML, Hahn-Windgassen A, Skeen J, Jacobs J, et al. Dwarfism, impaired skin development, skeletal muscle atrophy, delayed bone developement, and impeded adipogenesis in mice lacking Akt1 and Akt2. Genes Dev 2003; 17:1352-1365.

68. Schafer M, Farwanah H, Willrodt AH, Huebner AJ, Sandhoff K, Roop D, et al. Nrf2 links epidermal barrier function with antioxidant defense. EMBO Mol Med 2012; 4:364-379.

69. Huebner AJ, Dai D, Morasso M, Schmidt EE, Schafer M, Werner S, et al. Amniotic fluid activates the nrf2/keap1 pathway to repair an epidermal barrier defect in utero. Dev Cell 2012; 23:1238-1246.

Journal Pre-proof

Figure legends

Figure 1. Ric^{EKO} mice display a transient ichthyosis-like phenotype.

(A) Western blot analysis in epidermal isolates at P5. (B) Macroscopic appearance of littermates; boxed areas are shown at higher magnifications. (C) HE-stained back skin sections at P4 and quantification of epidermal thickness; e, epidermis; d, dermis; SC, stratum corneum; white dashed line indicates basal membrane, scale bar, 25 µm. (D) Quantification of TEWL at P4, each dot or square represents one mouse. (E) Body weight at P5. (F) Left: micrographs of isolated CE from back skin at P4. Right: quantification of the intact CE, each dot or square represents isolates from one mouse. (G) TEM image shows poorly condensed SC in Ric^{EKO} mice, note the presence of cell organelles in C1 of Ric^{EKO} mice (indicated by arrow). SG, stratum granulosum; C1, cornified layer 1, scale bar, 0.5 µm. Data are expressed as the mean; unpaired t-test was used to calculate *P* value; $^{**}P < 0.01$; $^{***}P < 0.001$.

Figure 2. Epidermal mTORC2 deficiency induces a compensatory transcriptional epidermal repair program in Ric^{EKO} mice.

(A) Volcano plot of differentially regulated transcripts between control and Ric^{EKO} epidermis at E19.5 (n=3 per genotype). Colored data points meet the thresholds of a $\log_2$ fold change of higher than 1 or lower than -1 and an adjusted *P* value of lower than 0.05. (B) GO of differentially regulated transcripts from Ric^{EKO} vs. control comparison using DAVID 6.8 online software. Only genes that have fold change >1.5 and a *P* value < 0.05 were used. (C) Log_2 fold changes of EDC gene expression in the epidermis of Ric^{EKO} skin. EDC genes with an alteration of fold change > 2 and and *P* value < 0.05 are shown.

(D) qRT-PCR analysis validation of differentially expressed genes from RNA-seq data in P0 epidermis (*n*=5/genotype). (E) Left: epidermal UV-response gene set enrichment plot in Ric^{EKO} samples. Right: heat map shows the stress-response genes with positive enrichment in Ric^{EKO} samples. All data are presented as mean ± s.e.m; unpaired t-test was used to calculate the *P* value; **P* < 0.05; ***P* < 0.01; ****P* < 0.001.

Figure 3. mTORC2 controls epidermal lipid metabolism.

(A) Fluorescent dye Nile red staining and quantification of back skin sections at P1(*n*=4); counterstained with DAPI; e, epidermis; d, dermis; white dashed line indicates basal membrane; scale bar, 25 μm. (B) Analysis of SC lipids by HPTLC (*n*=3 per genotype). Cer, ceramide; FFA, free fatty acid; Chol, cholesterol. (C) Left: GSEA of differentially regulated genes between control and Ric^{EKO} epidermis identifies enrichment of lipid and lipoprotein metabolism genes. Right: hierarchically clustered heat map illustration shows differential expression of lipid metabolism-related genes from RNA-seq data. (D) qRT-PCR analysis of *Elovl3* and *Pla2g5* in epidermis at P0 (*n*=5 per genotype). (E) Ultrastructural analysis of the interface between SG and SC at P5. Ric^{EKO} epidermis shows a disorganized interface (red arrows) between SG and SC, and displayed LB abnormalities, including disoriented lamellae and reduced lamellae number. In contrast, the LB of control showed regular lamellae orientation with equal distances lamellae (red bars). SG, stratum granulosum; C1, cornified layer 1; C2, cornified layer 2; LB, lamellar body, scale bar, 200 nm. All data are presented as mean ± s.e.m; unpaired t-test was used to calculate the *P* value; **P* < 0.05; ***P* < 0.01; ****P* < 0.001.

949 **Figure 4. Reduced proteolytic activity and impaired filaggrin processing in Ric^{EKO}**
950 **epidermis.**
951 (A) GSEA of RNA-seq data identifies enrichment of the (KEGG) lysosome gene set. (B)
952 Hierarchically clustered heat map shows altered expression of protease and protease
953 inhibitor genes. (C) qRT-PCR analysis of indicated genes at P0 (n=5). (D) qRT-PCR
954 analysis shows downregulated *Slpi* expression in Ric^{EKO} epidermis (n=5). (E) TEM
955 analysis shows delayed corneodesmosome degradation in Ric^{EKO} epidermis at P5.
956 Corneocyte layers (C) were numbered, arrows point to corneodesmosomes. SG, stratum
957 granulosum; scale bar, 200nm. (F) qRT-PCR analysis of epidermal filaggrin mRNA
958 expression at P5 (n=5). (G) Left, Western blot analysis at P5; Profilaggrin (Pro-FLG),
959 trimer (3F), dimer (2F) and monomer (1F) filaggrin are indicated. Right, quantified ratio
960 of filaggrin monomer (1F) and total filaggrin, Pro-filaggrin and β-actin with control set to
961 1 (n=4). All data are presented as mean ± s.e.m; unpaired t-test was used to calculate the
962 P value; *$P < 0.05$; **$P < 0.01$; ***$P < 0.001$.
963
964 **Figure 5. A keratinocyte-autonomous mTORC2-Akt axis controls filaggrin**
965 **processing.**
966 (A) Western blot analysis in cultured control and Ric^{EKO} keratinocytes, stimulated by
967 high concentration Ca^{2+} (0.2 mM). (B) Left, representative Western blot analysis in
968 keratinocytes; right, graph of relative densitometry of filaggrin trimer (3F), dimer (2F)
969 and monomer (1F). (C) Western blot analysis of filaggrin and Akt protein expression in
970 empty vector (control) and myr-Akt retrovirus infected control keratinocytes. (D) Left,
971 Western blot analysis in empty vector (control) and myr-Akt retrovirus infected Ric^{EKO}

keratinocytes; right, graph of relative densitometry of filaggrin trimer (3F), dimer (2F) and monomer (1F). All data are presented as mean ± s.e.m; unpaired t-test was used to calculate the *P* value; **P* < 0.05; ***P* < 0.01.

Figure 6. Epidermal mTORC2 determines immune cell composition in the skin.

(A) qRT-PCR profile in epidermis at P5 (*n*=8 per genotype). (B) Left: CD4 immunostaining on back skin sections at P5. Right: quantification of $CD4^+$ cells at high-power field (HPF). e, epidermis; d, dermis; white dashed line indicates basal membrane; scale bar, 25 µm. (C) Left: flow cytometry profile of γδ-TCR^+ $CD3^+$ cells at P5; right, percentage of different cell populations are shown at P5 (*n*=6 per genotype); cells were gated on 7-AAD^- $CD45^+$ skin cells. All data are presented as mean ± s.e.m; unpaired t-test was used to calculate the *P* value; **P* < 0.05; ***P* < 0.01; ****P* < 0.001.

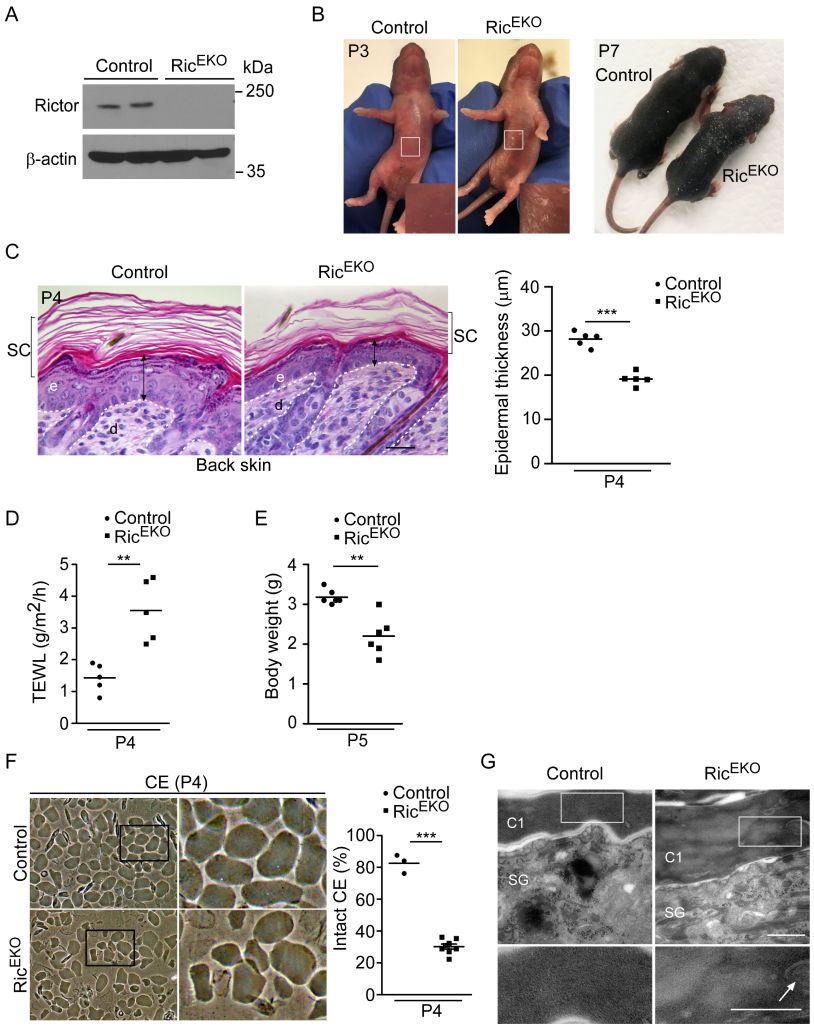
Figure 7. DETC number is reduced in Ric^{EKO} epidermis.

(A) Left: CD3 and γδ-TCR immunostaining on back skin at P5; Right: quantification of epidermal $CD3^+$ and γδ-TCR^+ cells per 500 µm of basement membrane; white dashed line indicates basal membrane; scale bar, 25 µm. (B) Hierarchically clustered heat map shows altered expression of *skint* family genes in Ric^{EKO} epidermis from RNA-seq data. (C) qRT-PCR analysis validates reduced *Skint1* and *Skint4* expression in Ric^{EKO} epidermis at P0 (*n*=5 per genotype). (D) Left: DETCs in epidermis of ear sheet at P70; separated epidermis was stained against γδ-TCR. Right: quantification of γδ-TCR^+ cells in the epidermal sheets. Scale bar, 25 µm. (E) Left: flow cytometry profile of single cell suspensions of ear skin at P70. 7-$AAD^-CD45^+CD3e^+$ cells were gated and analyzed for

995 expression of γδ-TCR and Vγ3-TCR, (right) quantification of γδ-TCR^{low}Vγ3-TCR^{-}
996 dermal γδ T cells and γδ-TCR^{high}Vγ3-TCR^{+} DETCs. (F) qRT-PCR analysis of *Skint1* and
997 *Skint4* expression in adult epidermis at P70 (*n*=5 per genotype). Each dot or square
998 represents one mouse. Data are presented as mean or as mean ± s.e.m; unpaired t-test was
999 used to calculate the *P* value; **P* < 0.05; ***P* < 0.01; ****P* < 0.001.
1000
1001 **Figure 8. Enhanced percutaneous immune response in Ric^{EKO} mice.**
1002 (A) DNFB-induced ACD response; right, H&E-staining of DNFB-treated ears. e,
1003 epidermis; d, dermis; c, cartilage, **P* < 0.05; ****P* < 0.001. (B) pAkt-S473
1004 immunofluorescent staining and morphometric quantification of pAkt-S473 stained
1005 unchallenged (0 h) and challenged (48 h) ear skin sections. (C) The number of
1006 eosinophils (Siglec F), mast cells (Giemsa), neutrophils (Gr1), macrophages (F4/80) and
1007 T cells (CD4 and γδ-TCR) per high power field (HPF, 400x) in unchallenged (0 h) and
1008 challenged ear (48 h) ear tissues. (D) Schematic diagram illustrating the proposed
1009 function of mTORC2 in regulating epidermal barrier function. Each dot or square
1010 represents one mouse. Data are presented as mean or as mean ± s.e.m; unpaired t-test or
1011 ANOVA one-way test analysis with Bonferroni multiple comparison test was used to
1012 calculate the *P* value; **P* < 0.05; ***P* < 0.01; ****P* < 0.001.
1013

Journal Pre-proof

Figure 1


A
Control
Ric^EKO
kDa
Rictor
250
β-actin
35
B
Control
Ric^EKO
P3
P7
Control
Ric^EKO
C
Control
Ric^EKO
P4
SC
SC
e
d
Back skin
Epidermal thickness (μm)
Control
Ric^EKO
***
P4
D
Control
Ric^EKO
**
TEWL (g/m2/h)
P4
E
Control
Ric^EKO
**
Body weight (g)
P5
F
CE (P4)
Control
Ric^EKO
Control
Ric^EKO
***
Intact CE (%)
P4
G
Control
Ric^EKO
C1
SG
C1
SG

Journal Pre-proof

Figure 2

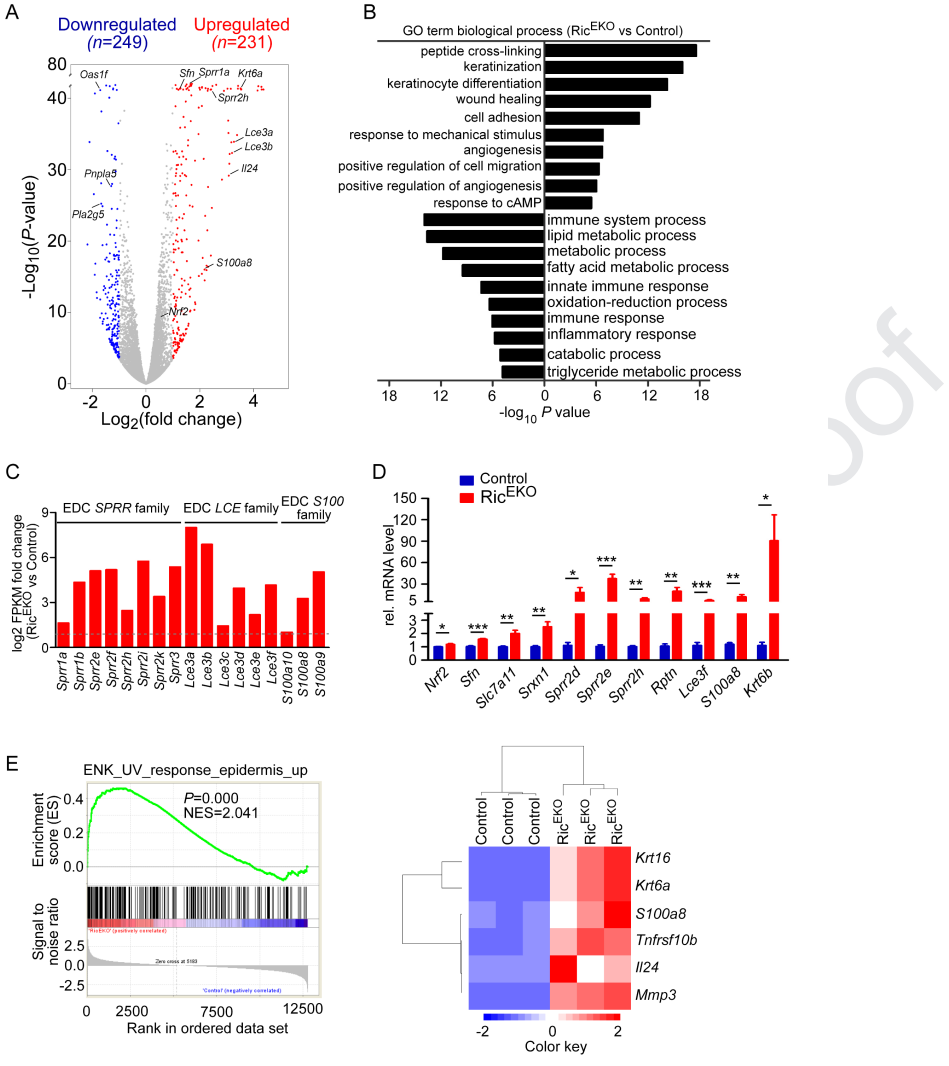


Figure 3

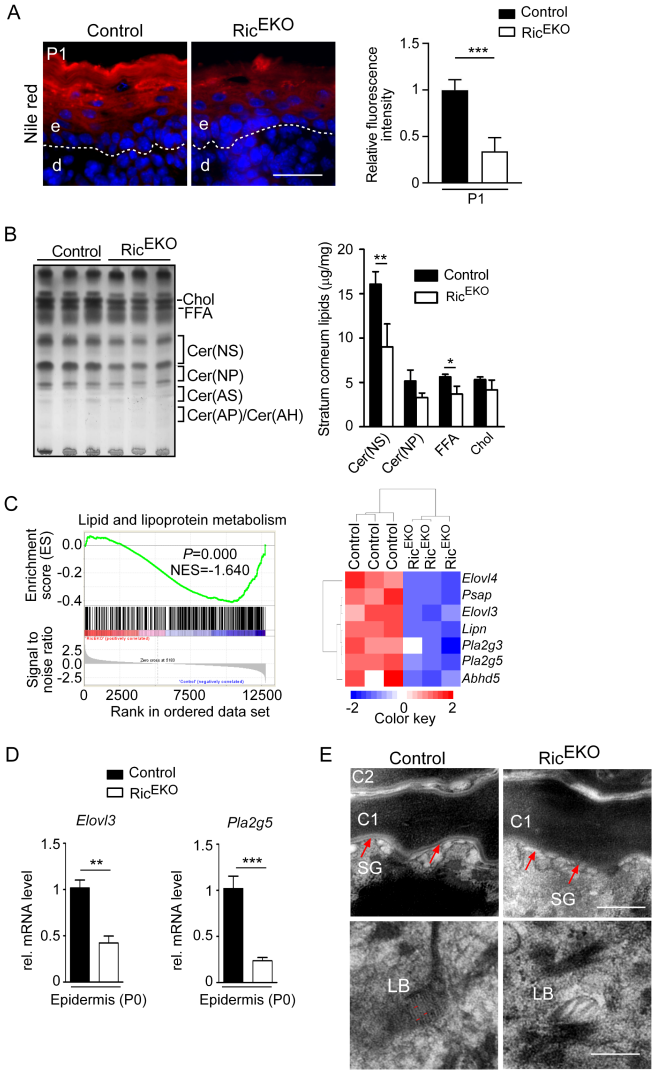

A
Control
RicEKO
P1
Nile red
e
d
Relative fluorescence intensity
***
B
-Chol
-FFA
Cer(NS)
Cer(NP)
Cer(AS)
Cer(AP)/Cer(AH)
Stratum corneum lipids (μg/mg)
**
*
Cer(NS)
Cer(NP)
FFA
Chol
C
Lipid and lipoprotein metabolism
Enrichment score (ES)
P=0.000
NES=-1.640
Signal to noise ratio
Rank in ordered data set
Elovl4
Psap
Elovl3
Lipn
Pla2g3
Pla2g5
Abhd5
Color key
D
Elovl3
Pla2g5
rel. mRNA level
Epidermis (P0)
E
C2
C1
SG
LB

Figure 4

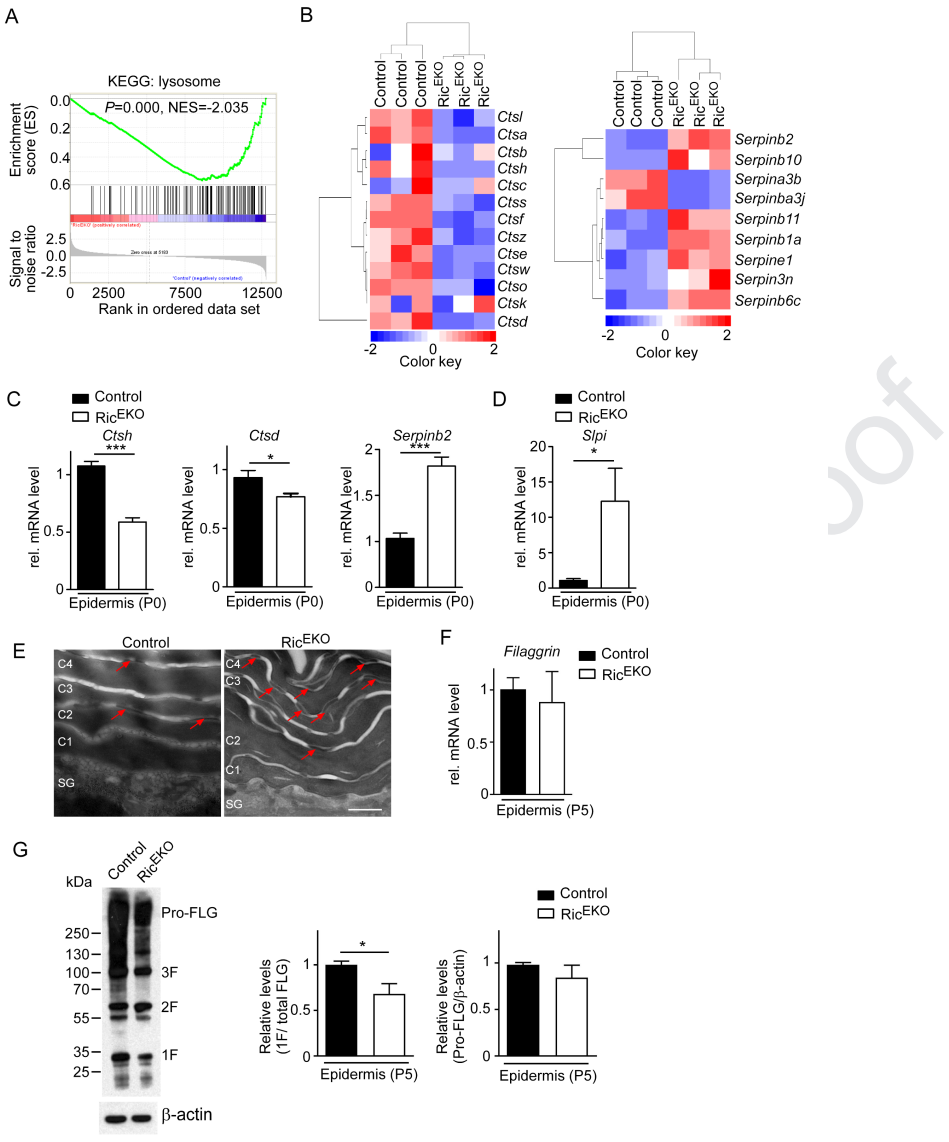

A
KEGG: lysosome
P=0.000, NES=-2.035
Enrichment score (ES)
Signal to noise ratio
Rank in ordered data set
B
Control
RicEKO
Ctsl
Ctsa
Ctsb
Ctsh
Ctsc
Ctss
Ctsf
Ctsz
Ctse
Ctsw
Ctso
Ctsk
Ctsd
Color key
Serpinb2
Serpinb10
Serpina3b
Serpinba3j
Serpinb11
Serpinb1a
Serpine1
Serpin3n
Serpinb6c
C
Ctsh
Ctsd
Serpinb2
rel. mRNA level
Epidermis (P0)
D
Slpi
E
C4
C3
C2
C1
SG
F
Filaggrin
Epidermis (P5)
G
kDa
Pro-FLG
3F
2F
1F
β-actin
Relative levels (1F/ total FLG)
Relative levels (Pro-FLG/β-actin)

Figure 5

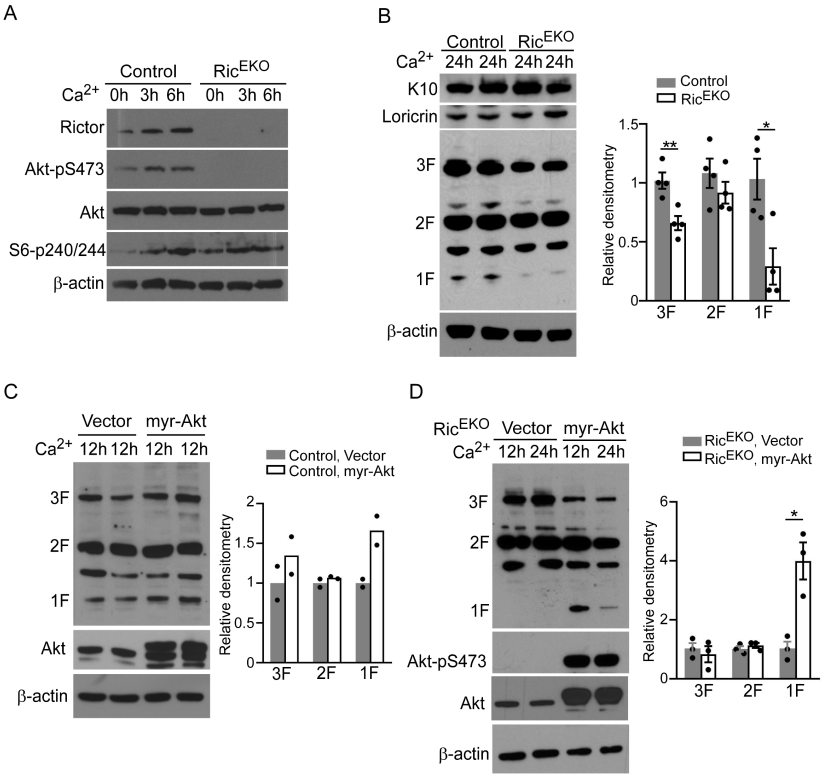

A
Control
RicEKO
Ca2+ 0h 3h 6h 0h 3h 6h
Rictor
Akt-pS473
Akt
S6-p240/244
β-actin
B
Control RicEKO
Ca2+ 24h 24h 24h 24h
K10
Loricrin
3F
2F
1F
β-actin
Control
RicEKO
Relative densitometry
3F 2F 1F
C
Vector myr-Akt
Ca2+ 12h 12h 12h 12h
3F
2F
1F
Akt
β-actin
Control, Vector
Control, myr-Akt
Relative densitometry
3F 2F 1F
D
RicEKO Vector myr-Akt
Ca2+ 12h 24h 12h 24h
3F
2F
1F
Akt-pS473
Akt
β-actin
RicEKO, Vector
RicEKO, myr-Akt
Relative densitometry
3F 2F 1F

Figure 6

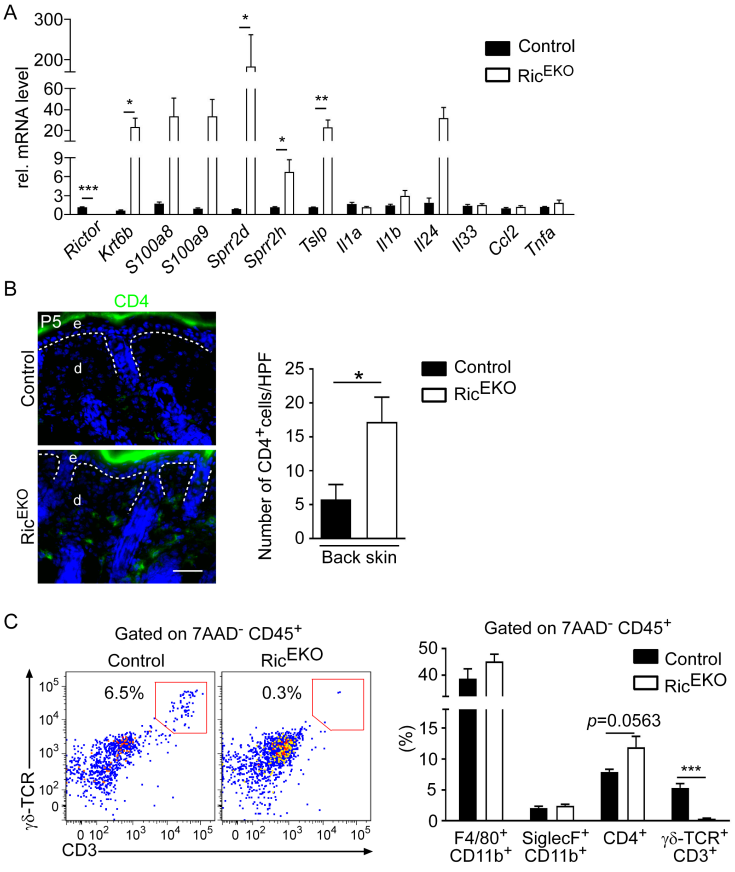

A
rel. mRNA level
Control
RicEKO
Rictor
Krt6b
S100a8
S100a9
Sprr2d
Sprr2h
Tslp
Il1a
Il1b
Il24
Il33
Ccl2
Tnfa
B
CD4
P5
e
d
Control
RicEKO
Number of CD4+cells/HPF
Back skin
C
Gated on 7AAD- CD45+
Control
RicEKO
6.5%
0.3%
γδ-TCR
CD3
p=0.0563
(%)
F4/80+ CD11b+
SiglecF+ CD11b+
CD4+
γδ-TCR+ CD3+

Figure 7

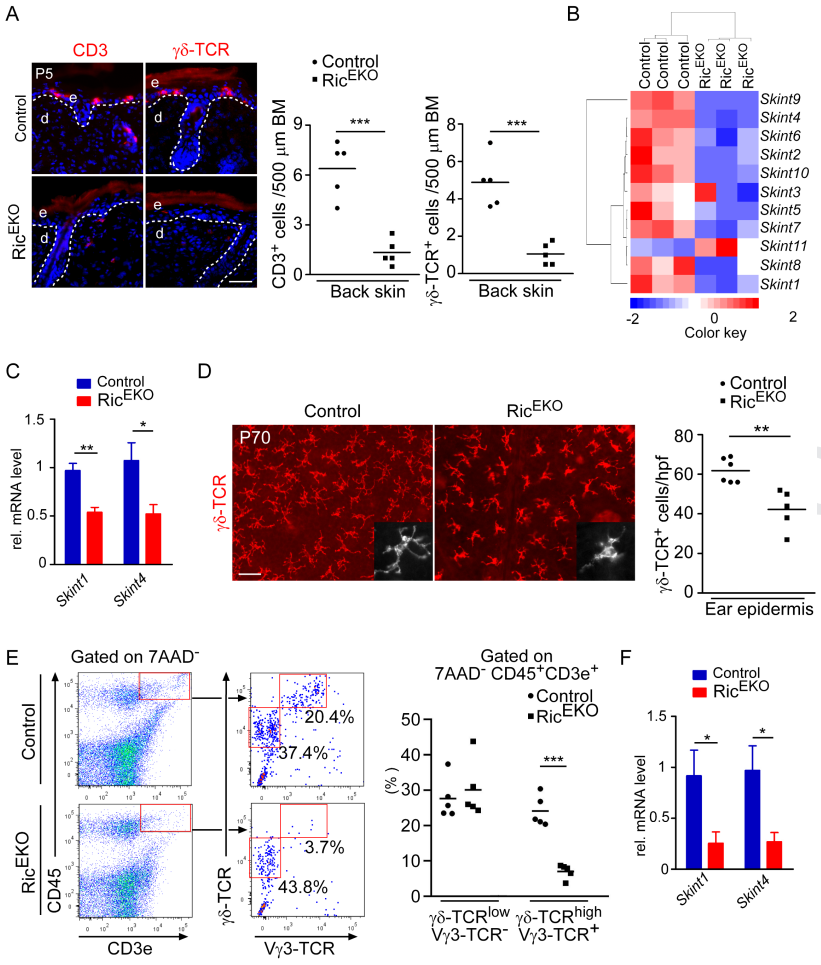
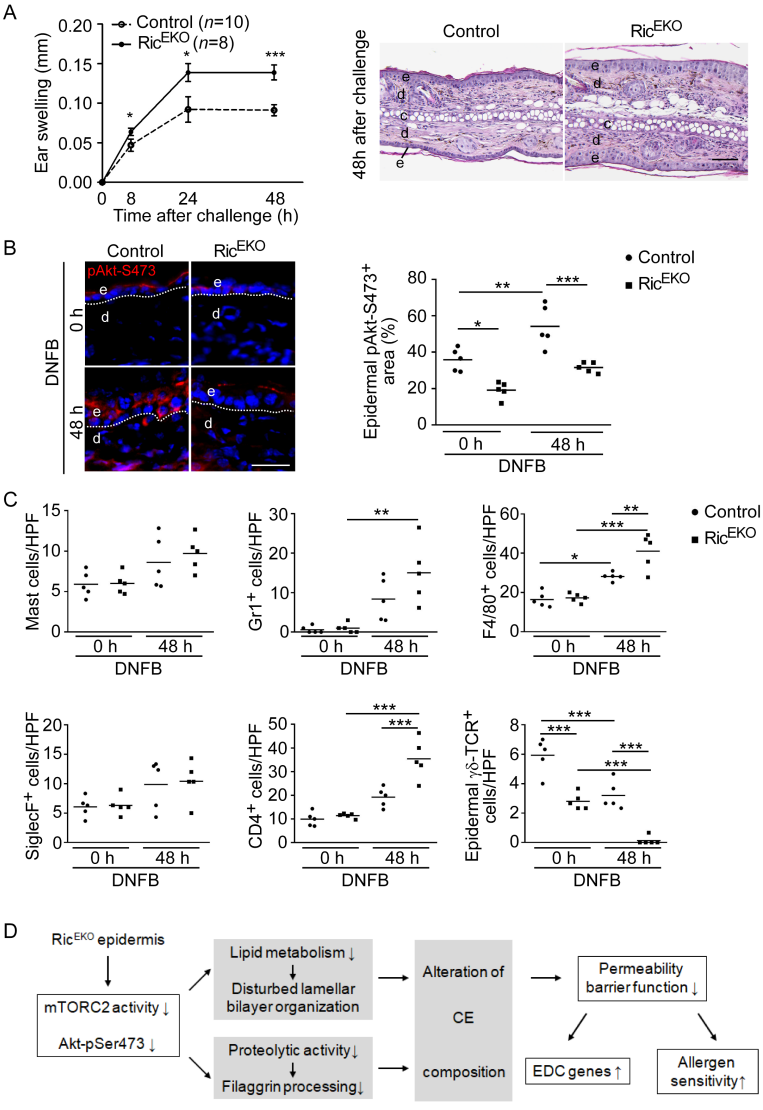

A
CD3
γδ-TCR
P5
Control
RicEKO
e
d
• Control
▪ RicEKO
CD3+ cells /500 μm BM
γδ-TCR+ cells /500 μm BM
***
Back skin
B
Control
Control
Control
RicEKO
RicEKO
RicEKO
Skint9
Skint4
Skint6
Skint2
Skint10
Skint3
Skint5
Skint7
Skint11
Skint8
Skint1
Color key
C
Control
RicEKO
rel. mRNA level
**
*
Skint1
Skint4
D
Control
RicEKO
P70
γδ-TCR
γδ-TCR+ cells/hpf
Ear epidermis
E
Gated on 7AAD-
Control
RicEKO
CD45
CD3e
γδ-TCR
Vγ3-TCR
20.4%
37.4%
3.7%
43.8%
Gated on
7AAD- CD45+CD3e+
(%)
γδ-TCRlow
Vγ3-TCR-
γδ-TCRhigh
Vγ3-TCR+
F
Control
RicEKO
rel. mRNA level
Skint1
Skint4

Figure 8


A
Control (n=10)
RicEKO (n=8)
Ear swelling (mm)
Time after challenge (h)
Control
RicEKO
48h after challenge
B
Control
RicEKO
pAkt-S473
DNFB
0 h
48 h
Epidermal pAkt-S473+ area (%)
C
Mast cells/HPF
Gr1+ cells/HPF
F4/80+ cells/HPF
SiglecF+ cells/HPF
CD4+ cells/HPF
Epidermal γδ-TCR+ cells/HPF
D
RicEKO epidermis
mTORC2 activity ↓
Akt-pSer473 ↓
Lipid metabolism ↓
Disturbed lamellar bilayer organization
Proteolytic activity ↓
Filaggrin processing ↓
Alteration of CE composition
Permeability barrier function ↓
EDC genes ↑
Allergen sensitivity ↑

Journal Pre-proof

Online Repository

Epidermal mTORC2 controls lipid synthesis and filaggrin processing in epidermal barrier formation

Xiaolei Ding, PhD [1,2], Sebastian Willenborg, PhD[1], Wilhelm Bloch, PhD [3], Sara A. Wickström, MD, PhD [4,5,6,7], Prerana Wagle, MSc [7], Susanne Brodesser, PhD [7], Axel Roers, MD [8], Alexander Jais, PhD [9], Jens C. Brüning, MD [2,7,9], Michael N. Hall, PhD [10], Markus A. Rüegg, PhD [10], Sabine A. Eming, MD [1,2,7]

[1]Department of Dermatology, University of Cologne, Kerpenerstr. 62, 50937 Cologne, Germany

[2]Center for Molecular Medicine Cologne (CMMC), University of Cologne, 50931 Cologne, Germany

[3]Department of Molecular and Cellular Sport Medicine, German Sport University Cologne, 50933 Cologne, Germany

[4]Paul Gerson Unna Group 'Skin Homeostasis and Ageing', Max Planck Institute for Biology of Ageing, 50931 Cologne, Germany

[5]Helsinki Institute of Life Science, Biomedicum Helsinki, University of Helsinki, FI-00014 Helsinki, Finland

[6]Wihuri Research Institute, Biomedicum Helsinki, University of Helsinki, FI-00014 Helsinki, Finland

[7]Cluster of Excellence Cellular Stress Responses in Aging-associated Diseases (CECAD), University of Cologne, 50931 Cologne, Germany

Journal Pre-proof

Journal Pre-proof

[8]Institute for Immunology, Medical Faculty Carl Gustav Carus, TU Dresden, 01307 Dresden, Germany

[9]Max Planck Institute for Metabolism Research, Gleueler Strasse 50, 50931 Cologne, Germany

[10]Biozentrum, University of Basel, CH-4056 Basel, Switzerland

Corresponding author:

Sabine A. Eming, MD

Professor of Dermatology

Department of Dermatology

University of Cologne

Kerpenerstr. 62

50937 Cologne

Germany

Phone: ++49-221-4783196

Fax: ++49-221-4785949

E-mail: sabine.eming@uni-koeln.de

Journal Pre-proof

Journal Pre-proof

Supplemental Materials

Supplemental Figure 1. Conditional targeting *Rictor* gene in epidermal keratinocytes.

Supplemental Figure 2. Immune cell composition and gating strategies for FACS analysis of cell suspensions isolated from back skin and ear.

Supplemental Figure 3. Mild skin inflammation in naïve Ric^{EKO} mice under SPF conditions.

Supplemental Figure 4. Immune cell infiltration in ear skin tissue.

Supplemental Figure 5. Gene expression analysis in ear skin tissue.

Supplemental Table 1: Antibodies used for immunostaining and Western blot analysis

Supplemental Table 2: Primer sequence used for qRT-PCR analysis

Supplemental Table 3: Genes in biological processes (BP) identified by GO term analysis.

Journal Pre-proof

Journal Pre-proof

Supplemental Figure legends

Supplemental Figure 1. Conditional targeting *Rictor* gene in epidermal keratinocytes.

(A) Scheme illustrating the *Rictor* gene construct, the 2 loxP sites flanking exons, and the PCR fragment length before and after recombination. (B) PCR product of genomic DNA isolated from various tissues. (C) Phospho-Akt (Akt-pS473) immunostaining of back skin of control and Ric^{EKO} at P5; scale bar, 25 µm. (D) Survival curve of control (*n*=16) and Ric^{EKO} (*n*=15) mice. Mantel-Cox test was used to calculate the P value. (E) Representative H&E-stained back skin sections from control and Ric^{EKO} mice at P70. Scale bar, 25 µm. (F) TEWL in Ric^{EKO} and control mice. (G) Representative immunofluorescence staining at P5 for ZO-1, E-cadherin (E-cad), Desmoplakin1/2 (DSP1/2), Desmoglein1/2 (DSG1/2), β4-integrin (red); white dashed lines indicates basement membrane; nuclei are visualized with DAPI (blue); scale bar, 20 µm. (H) Body weight of control (*n*=8) and Ric^{EKO} (*n*=7) mice at different ages. (I) Ultrastructural analysis of back skin epidermis of control and Ric^{EKO} mice at P5. Lower panel: higher magnification images show desmosome (de) structure. e, epidermis; d, dermis; SC, stratum corneum; SG, stratum granulosum; SS, stratum spinosum; SB, stratum basale, scale bar, 5 µm (upper panel) and 100 nm (lower panel). Each dot or square represents one mouse. Data are presented as mean or as mean ± s.e.m; unpaired t-test was used to calculate the *P* value; $^{**}P < 0.01$; $^{***}P < 0.001$.

Supplemental Figure 2. Immune cell composition and gating strategies for FACS analysis of cell suspensions isolated from back skin and ear.

(A) Left: Representative Giemsa staining and F4/80 immunostaining with back skin sections from control and Ric^{EKO} mice at P5. Right: quantification of mast cells and $F4/80^{+}$ macrophages cells per high-power field (HPF) (*n*=5 per genotype). Scale bar, 25 µm; data are presented as as mean ± s.e.m. (B) Representative FACS analysis of single cell suspensions of back skin in control and Ric^{EKO} mice (P5). Upper panel: single cells were gated (G1-3) and analyzed for 7-AAD staining and expression of CD45 (G4). Lower panel: $7\text{-}AAD^{-}CD45^{+}$ cells (G4) were analyzed for expression of (from left to right) CD3 and γδ-TCR, CD4, CD11b and F4/80, and CD11b and Siglec F. (C) Representative FACS analysis of single cell suspensions of ear skin in control and Ric^{EKO} mice (P70). Single cells (G1-3) and $7\text{-}AAD^{-}$ cells (G4) were gated. Red polygons indicate the gate and percentages indicate the proportion of gated cells. FSC-A, forward scatter area; FSC-H, forward scatter height; G, gate; SSC-A, sideward scatter area; SSC-H, sideward scatter height.

Supplemental Figure 3. Mild skin inflammation in naïve Ric^{EKO} mice under SPF conditions.

(A) Representative macroscopic appearance of control and Ric^{EKO} mice at P70. (B) Quantification of $CD4^{+}$, mast cells (MCs), and $F4/80^{+}$ macrophages in back skin sections from control and Ric^{EKO} mice at P70 (*n*=5 per genotype). (C) qRT-PCR analysis of *Il6*, *Tnfα*, *Il1b,* and *Tslp* expression in Ric^{EKO} and control skin at P70 (*n*=5 per genotype). (D) Serum IgE amount in Ric^{EKO} and control mice were determined by ELISA (*n*=6 per

genotype) at P70. (E) Croton oil-induced irritated contact dermatitis (ICD) response. Ear swelling of control and Ric^{EKO} animals after topical application of croton oil was calculated and shown (*n*=5 per genotype). Data are presented as mean ± s.e.m.

Supplemental Figure 4. Immune cell infiltration in ear skin tissue. Representative Giemsa stainings and immunohistochemical stainings for Gr1, F4/80, Siglec F, CD4 and γδ-TCR of untreated (DNFB, 0 h) and treated (DNFB, 48 h) ear sections from control and Ric^{EKO} mice (*n*=5). Arrows indicate mast cells (Giemsa stain, purple) or polymorphonuclear cells (Gr1 stain, brown) and dashed line indicates the border between epidermis and dermis. e, epidermis; d, dermis; scale bar, 25 µm.

Supplemental Figure 5. Gene expression analysis in ear skin tissue.

qRT-PCR analysis of stress response gene (*Krt6b*, *S100a8* and *Sprr2d*) and inflammatory mediator (*Il6, Tnfa* and *Il24*) expression in untreated (DNFB, 0 h) and treated (DNFB, 24 h) ear skin tissues from control and Ric^{EKO} mice (*n*=6 per genotype). Gene expression in untreated control ear skin was referred as 1 and relative fold changes were analyzed and shown. Data are presented as mean ± s.e.m; ANOVA one-way test analysis with Bonferroni multiple comparison test was used; **P* < 0.05; ***P* < 0.01; ****P* < 0.001.

Supplemental Table 1: Antibodies used for immunostaining and Western blot analysis

Name	*Catalog number*	*Source*
Primary antibodies used for immunostaining		
Akt-pS473	9271	Cell Signaling, Beverly, MA
CD4	14-0042-85	Thermo Fisher Scientific
Ly-6G and Ly-6C (Gr1)	550291	BD Biosciences
Siglec F	552126	BD Biosciences
CD3	MCA1477	AbD Serotec
F4/80	MOF4F (V500)	Dianova
ZO-1	(hybridoma) Rat, Clone R26.4C Stevenson BR et al., 1986	
Desmoglein1/2	61002	Progen
Desmoplakin1/2	61003	Progen
β4-integrin	555719	BD Biosciences
E-cadherin	610182	BD Biosciences
γδ T-Cell Receptor	553175	BD Biosciences
Secondary antibodies used for immunostaining		
Anti-rabbit IgG Alexa Fluor® 488	A-32731	Thermo Fisher Scientific
Anti-rabbit IgG Alexa Fluor® 568	A-11011	Thermo Fisher Scientific
Anti-rat IgG Alexa Fluor® 488	A-11006	Thermo Fisher Scientific
Anti-mouse Alexa Fluor® 594	A-11032	Thermo Fisher Scientific
Anti-rabbit IgG HRP	K4003	DAKO

Journal Pre-proof

Primary antibodies used for Western blot		
S6-pS240/244	5364	Cell Signaling, Beverly, MA
Rictor	2140	Cell Signaling, Beverly, MA
Akt-pS473	9271	Cell Signaling, Beverly, MA
Loricrin	PRB-145P	Covance, Princeton, New York
Filaggrin	PRB-417P	Covance, Princeton, New York
Akt	9272	Cell Signaling, Beverly, MA
Keratin 10	PRB-159P	Covance, Princeton, New York
β-actin (C4)	MAB1501	Sigma-Aldrich
α-Tubulin (B-5-1-2)	T6074	Sigma-Aldrich
Secondary antibodies used for Western blot		
Anti-rabbit-IgG-HRP	P0448	DAKO
Anti-mouse-IgG-HRP	P0161	DAKO

Journal Pre-proof

Supplemental Table 2: Primer sequence used for qRT-PCR analysis

Gene	*Forward primer*	*Reverse primer*
GAPDH	CATGTTTGTGATGGGTGTGA	AATGCCAAAGTTGTCATGGA
Nrf2	CCATTCCCGAATTACAGTGTCTTA	CGCCAAAATCTGTGTTTAAGGTG
Sfn	CCGAACGGTATGAAGACATGG	CGGTACTTTCACCTCGGG
Slc7a11	CAACAAAGATCGGGACTGCT	GCTGGCTGGTTTTACCTCAA
Srxn1	CGGTGCACAACGTACCAAT	TTGATCCAGAGGACGTCGAT
Sprr2d	CTGGTACTCAAGGCCGAGAC	CAGGGCACTTTGGTGGAG
Sprr2e	CAGGTCCTAGGCTACTTTGGAG	ACTGTGGATGAGGACAAGGC
Sprr2h	GACACTTGGTACTCAAGCTCTGG	TGCACTGCTGCTGTTGGTAA
Rptn	TCCTGCCTCTTCTGCTCATT	AGCGCCTACCCCATGATATT
Lce3f	TCCTGGCTCTTCCTGTTCTC	CCCAGGCAGTTATCAAAAGC
S100a8	GCCGTCTGAACTGGAGAAG	GTGAGATGCCACACCCACTT
Keratin6b	TGCAGACGAGATCAACTTCC	TGCAGACGAGATCAACTTCC
Elovl3	CTGTTGCTCATCGTTGTTGG	GCTTGAGGCCCACTGTAAAC
Pla2g5	CTCACACTGGCTTGGTTCCT	CATAACAACGGTCGTGCATC
Ctsh	CACGGAGACGGAGTTACCAG	GTGGCCATTACACTCCTGCT

Ctsd	AATCCCTCTGCGCAAGTTCA	CACTGGCTCCGTGGTCTTAG
Slpi	CGGCAAATACAAGTGCTGTG	CCTGGGAGCAGGGAAGTAGT
Serpinb2	TGCCAGCTTTCCAAGAAGCATT	AGATTGAGGGCAAACATGGTG
Rictor	GAGAAAGCTGGGCCATCTGA	AACCCGGCTGCTCTTACTTC
Tslp	TCTCAGGAGCCTCTTCATCCT	CTCACAGTCCTCGATTTGCTC
Il-1α	GTCGGGAGGAGACGACTCTA	TGGTCACAAACAGTGGGAGG
Il-1β	GGACCCCAAAAGATGAAGGGCTGC	GCTCTTGTTGATGTGCTGCTGCG
Il-24	TGCCAAGTGACAGGGGTGGTTCT	CAGCACCCGAGACATTCCGCAG
Il-33	TGATCAAAGAGGCCGGGAAC	ACGCAGATTCCGCCTTTACA
Ccl2	TCCACGTGTTGGCTCAGCCAG	CCAGCCTACTCATTGGGATCATCTT
Tnf-α	GACCCTCACACTCAGATCATCTTCT	CCTCCACTTGGTGGTTTGCT

Supplemental Table 3. Related to Figure 3. Differentially expressed genes in GO term analysis identified biological processes (BP). Gene ontology Enrichment analysis (GO) of differentially regulated transcripts from Ric^{EKO} vs. control comparison using DAVID 6.8 online software. Only genes that have fold change >1.5 and a *P* value < 0.05 were used.

BP	Up-regulated genes in Ric^{EKO} epidermis
Peptide cross-linking	LCE3A, LCE3B, LCE3C, COL3A1, LCE3D, SPRR2H, SPRR2F, SPRR2E, SPRR2K, SPRR2I, LCE1J, SPRR2D, SPRR1A, SPRR2A3, SPRR1B, SPRR2B, TGM1, SPRR2A2, SPRR3, LCE3F, LCE3E, THBS1, LCE1K
Keratinization	KRT6A, KRT6B, SPRR2H, SPRR2F, SFN, SPRR2E, SPRR2K, SPRR2I, KRT17, KRT16, SPRR2D, SPRR1A, SPRR2A3, SPRR1B, CNFN, SPRR2B, TGM1, SPRR2A2, SPRR3
Keratinocyte differentiation	PTGS2, LCE3A, LCE3B, LCE3C, LCE3D, SPRR2H, SPRR2F, SFN, SPRR2E, SPRR2K, SPRR2I, LCE1J, KRT16, SPRR2D, SPRR1A, SPRR2A3, SPRR1B, SPRR2B, TGM1, SPRR2A2, SPRR3, LCE3F, LCE3E, LCE1K
Wound healing	DCBLD2, KRT6A, NOG, S100A8, TNC, COL3A1, CXCL2, TGFBR2, IL24, ELK3, AQP1, TPM1, MMP12, TIMP1, MACF1, CCL20, SERPINE1, SERPINB2, TGFA, CNN2, LOX, COL1A1, NBEAL2
Cell adhesion	CADM4, VCL, NOV, CGREF1, COL12A1, CYR61, KIRREL3, BYSL, CDHR1, ADGRE5, FBLIM1, THY1, TNFAIP6, BVES, HAS1, VCAN, LAMC2, MFAP4, TNFRSF12A, TNC, ITGB4, ITGB1, DCHS1, PTK2B, ITGB6, COL6A2, COL6A1, THBS1, THBS2, THBS3, DPT, COL18A1, PODXL, ITGA3, TINAGL1, PCDH17, COL5A1, LYVE1, COL19A1, CASS4, ITGA6, ITGA5, DSG3, PKP4, ITGA7, SULF1, DSC2, ABL2, NTM, MYH10

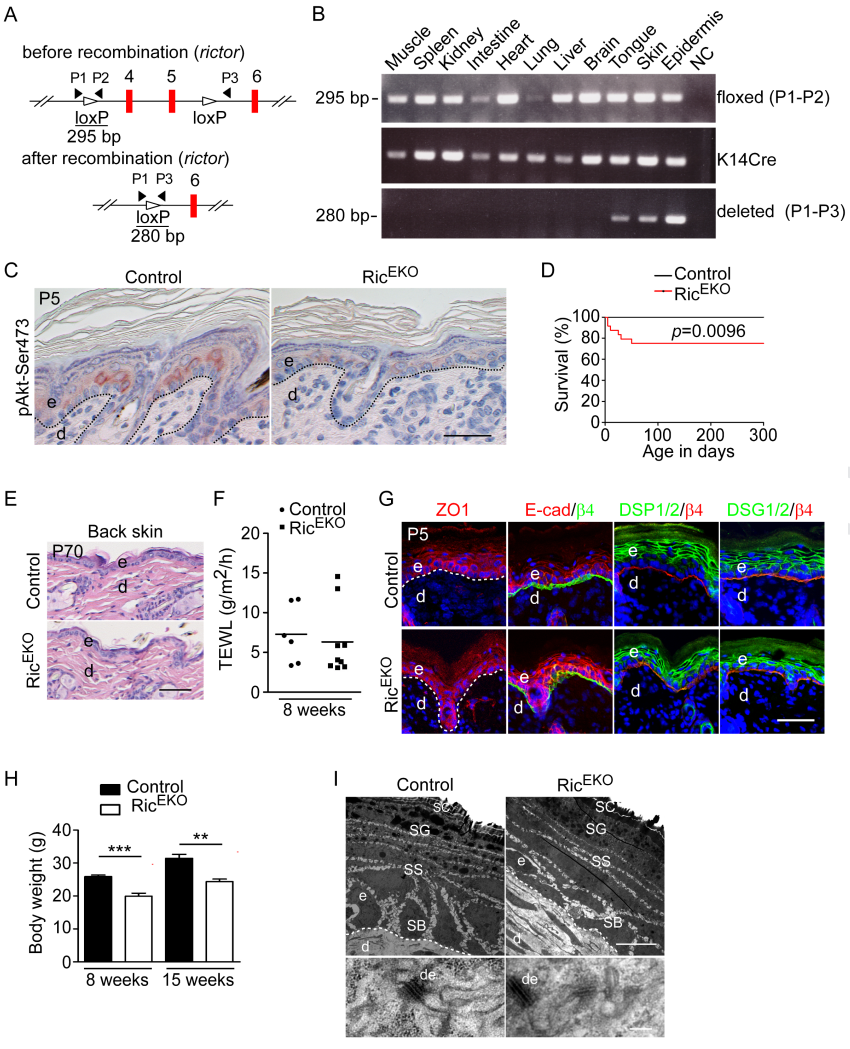
BP	Down-regulated genes in Ric^{EKO} epidermis
Immune system process	LY86, TLR1, LY9, C1QC, SKAP1, ISG20, TLR9, OASL2, OASL1, CLEC4A2, CD300C2, CD3E, PRG2, PIK3CD, PADI4, TRAT1, CD84, C1QA, C1QB, H2-AA, CD300LF, TXK, RNF135, TNFAIP8L2, KLRK1, UNC93B1, SP110, OAS2, IL34, RNF125, NAIP5,

	PSTPIP1, ZAP70, MR1, CSF1R, CD7, ZBP1, ITK, CARD9, THEMIS, HCK, TNFRSF13C, CTLA4, TRIL, FCGR1, PSMB9, IFIT3, LAT, IFIT2, H2-EB1, C1RL, THEMIS2
Lipid metabolic process	ACOX2, PPARA, ALOX12E, HINT2, BSCL2, 4833423E24RIK, GPCPD1, ACOX3, FAR2, INSIG2, APOE, ELOVL3, NPC1L1, CES1D, FA2H, PLD4, DECR1, LPCAT2, PNPLA5, HSD11B1, NEU3, THEM5, AKR1D1, PLA2G5, HACL1, ECH1, HSD17B2, ABHD3, CERS4, ACSBG1, PLIN5, ACSL4, ACAA1B, GAL3ST1, ACSL6, SCD1, SOAT1, PLA2G16, SCD3, A4GALT, PLB1, CYP46A1, ACER2, ACER1, FADS3, SPTSSB, FAM213B, ACACB, CRAT, FADS6, GDPD1, AWAT2, ACSM3, AWAT1, ACSM2, ACSM1, LIPC
Metabolic process	ACOX2, ARSB, ALAD, ARSG, HEXB, ECHDC1, GM436, ACOX3, UGT1A7C, UGT1A6B, PHOSPHO1, 9430007A20RIK, ACOXL, NEIL2, FBP1, ALDH3B2, LPCAT2, UGT1A1, PNPLA5, AADAC, CAMK1, NEU3, ALPL, ECH1, GM5538, ISOC2B, HSD3B6, UGT3A1, UGT3A2, ACSBG1, C130079G13RIK, ALDH1A1, ALDH1A7, ACSL4, ACAA1B, FAHD2A, ACSL6, GSTA2, GSTA3, ACY3, PM20D1, NPL, GM13124, ACACB, ENGASE, CPS1, ACSM3, ACSM2, ACSM1, LYG2, ARSA, GM13178, GM13177, ACAD10
Fatty acid metabolic process	ACOX2, PPARA, ECH1, ALOX12E, 4833423E24RIK, ACSBG1, ACOX3, CRYL1, ELOVL3, ACSL4, ACAA1B, ACSL6, SCD1, SCD3, ACOXL, FA2H, FADS3, FAM213B, ACACB, DECR1, CRAT, FADS6, ACSM3, ACSM2, ACSM1, LIPC, THEM5
Innate immune response	TNFAIP8L2, LY86, TLR1, KLRK1, UNC93B1, SP110, TRIM15, OAS2, LY9, IL34, C1QC, TLR9, ISG20, OASL2, NAIP5, OASL1, ZAP70, PSTPIP1, FCER1G, CLEC4A2, MR1, CSF1R, TYROBP, ZBP1, ITK, CARD9, HCK, PIK3CD, PADI4, TRIL, FCGR1, IFIT3, CD84, C1QA, IFIT2, C1QB, CYBB, C1RL, TXK, TREM2, RNF135

Journal Pre-proof

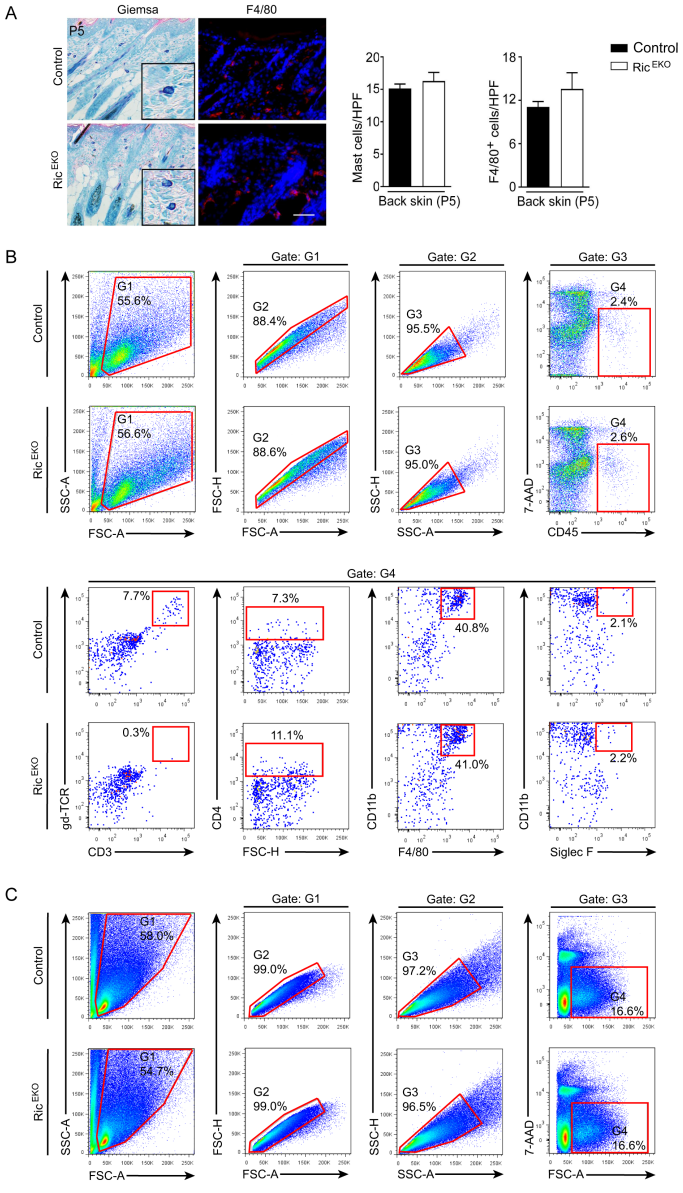
Journal Pre-proof

Supplemental Figure 1

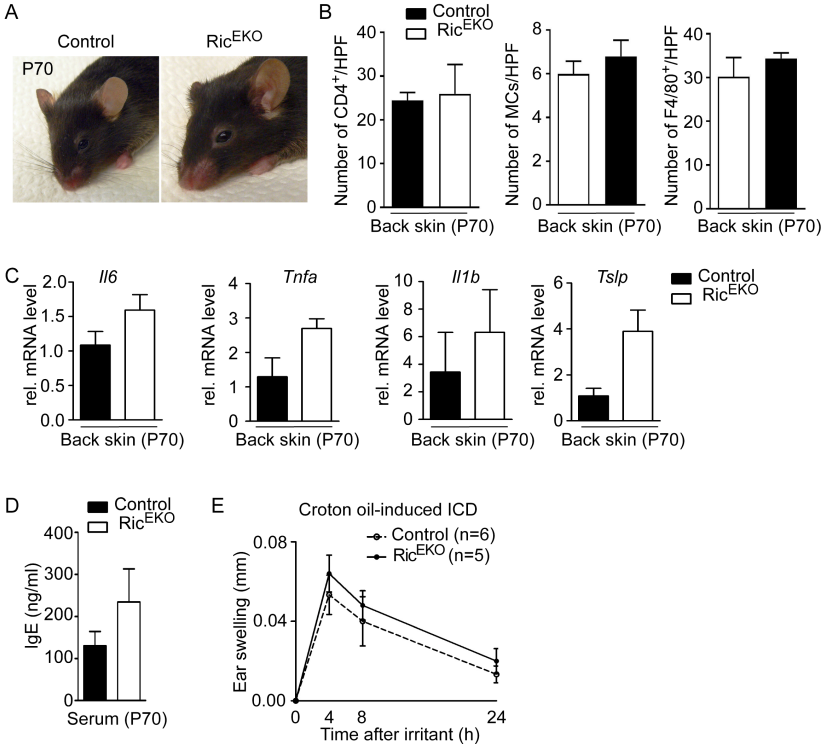


Journal Pre-proof

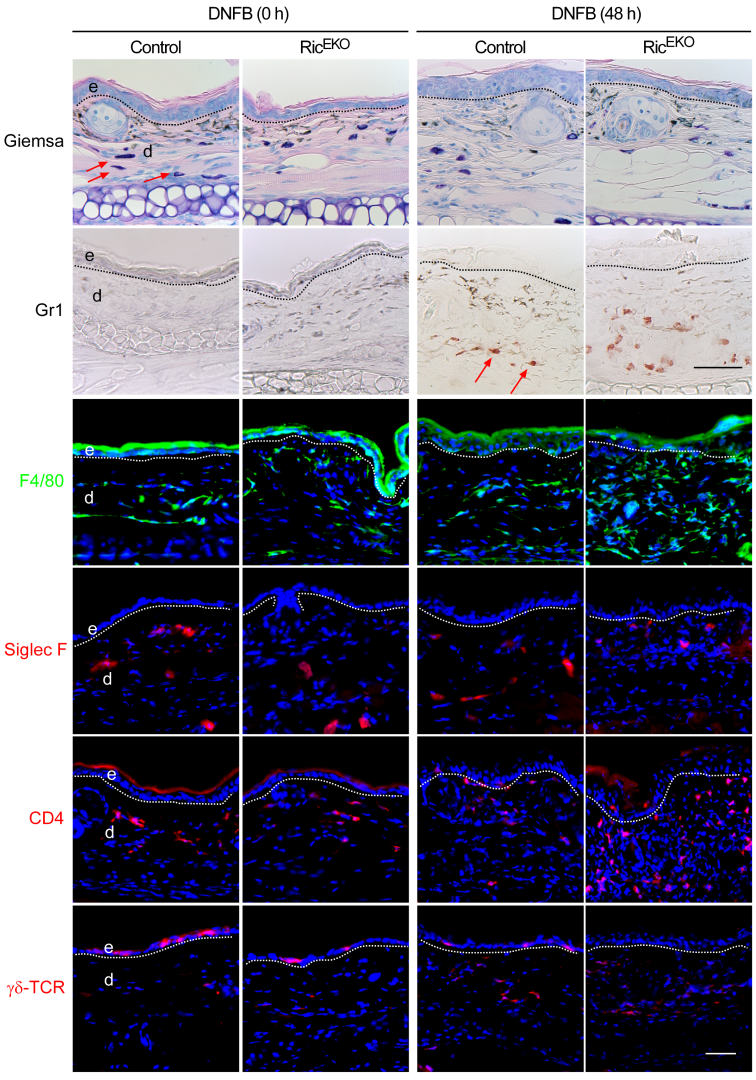
Supplemental Figure 2



Supplemental Figure 3



Supplemental Figure 4



Supplemental Figure 5

